1 Volcanological context of the 2022 Hunga eruption

Lead authors	Simon Carn Anja Schmidt
Co-authors	Kristen Fauria Corinna Kloss Isobel Yeo
Contributing authors	Larry Mastin Tjarda Roberts

Cite this as:

Carn, S., A. Schmidt et al. (2025): Volcanological context of the 2022 Hunga eruption. In APARC, 2025: The Hunga Eruption Atmospheric Impacts Report [Yunqian Zhu, Graham Mann, Paul A. Newman, William Randel (Eds.)]. APARC Report No. 11, WCRP Report No. 10/2025, DOI: 10.34734/FZJ-2025-05238, available at `https://aparc-climate.org/publications/aparc-report-no-11/`.

Key points

- **The 15 January 2022 eruption of Hunga volcano (Kingdom of Tonga) was a submarine explosive eruption that may represent the first geophysically-observed example of a 'phreatoplinian' event.** A phreatoplinian event is a high-magnitude explosive volcanic eruption involving the interaction of magma and external water. This renders the Hunga eruption unique in the era of satellite observations and distinct from large eruptions of recent decades that were subaerial (e.g., 1982 El Chichón, 1991 Pinatubo).

- **Hunga provides the first direct observations of substantial stratospheric hydration by a submarine eruption.** Stratospheric injection of large quantities of water vapour by volcanic eruptions has been hypothesised in the past, but never directly observed. The Hunga eruption also provides evidence for atmospheric injection of sea salt derived from evaporated seawater.

- **Hunga volcano was persistently active in the century prior to the 2022 eruption.** This is unusual for volcanoes that produce major eruptions, which are usually dormant for decades to centuries prior.

- **The 15 January 2022 Hunga eruption was preceded by a month of precursory unrest.** This included two other significant explosive eruptions on 19 December 2021 and 13 January 2022. Weeks to months of precursory unrest is typical of major volcanic eruptions.

- **The 15 January 2022 eruption of Hunga provided a wealth of correlated, geophysical observations of a high-magnitude, phreatomagmatic eruption.** Satellite measurements of umbrella cloud growth rates, lightning detection, explosion and atmospheric wave detection, tsunami inundation records, and bathymetric mapping of deposits combine to yield an unprecedented dataset for a potentially phreatoplinian eruption.

- **The 2022 Hunga eruption had a Volcanic Explosivity Index (VEI) of 6, equal to the 1991 Pinatubo eruption.** Most of the Hunga eruption products were emplaced underwater by submarine volcaniclastic density currents, complicating assessments of eruption magnitude. Future refinements of eruption magnitude are likely as bathymetric investigations continue at Hunga.

- **Hunga's sulfur dioxide (SO_2) emissions (~0.5-1 Tg) were at least an order of magnitude less than Pinatubo.** This is well below the ~5 Tg SO_2 threshold required for significant climate impacts due to sulfate aerosols. The Hunga magma may have degassed up to ~20 Tg SO_2 during the eruption, but the majority did not reach the atmosphere.

- **Rapid response to the Hunga eruption from the volcanological and atmospheric science communities collected critical data.** Rapid tephra sampling enabled characterisation of the magma composition and volatile budget. Balloon sondes were able to sample the stratospheric Hunga plume downwind 7-10 days after the eruption. Rapid response cruises to collect bathymetric data provided critical observations of submarine deposits for eruption magnitude assessment.

- **Stratospheric aerosol perturbations by volcanic eruptions and extreme wildfires were frequent in the decade prior to the 2022 Hunga eruption.** At the time of the Hunga eruption in January 2022, the stratospheric aerosol optical depth was approximately double the baseline value.

- **Although the 15 January 2022 Hunga eruption was strongly influenced by the interaction of magma and seawater, the precise role of seawater in driving the eruption is a fundamental question yet to be resolved.** Future, detailed analysis of predominantly submarine tephra samples (challenging to access) will provide further insight into volcanic processes.

- **The 2022 Hunga eruption is by far the largest of several recent explosive eruptions that also produced water-rich, upper tropospheric and stratospheric plumes.** If modest SO_2 emissions are characteristic of these events, they may be poorly preserved in ice core proxy records of prehistoric eruptions.

- **The closest historical analog to the 2022 Hunga eruption is the August 1883 Krakatau eruption (Indonesia).** The Hunga and Krakatau eruptions both produced multiple paroxysmal explosions, globally detected atmospheric waves and tsunamis, submarine calderas and extensive submarine pyroclastic density current deposits. Comparisons of the Hunga and Krakatau eruptions should improve our understanding of the 1883 event.

- **The frequency of explosive submarine eruptions similar to or larger than the 2022 Hunga eruption prior to the instrumental era is unknown.** However, emerging research on submarine volcanism in Tonga and elsewhere suggests that submarine eruptions of a similar magnitude to Hunga may be more common in the geological record than previously recognised. More extensive and detailed seafloor bathymetry and geological studies are needed to elucidate the frequency and potential hazards of future Hunga-like eruptions.

Contents

Preamble

Large volcanic eruptions that inject material into the stratosphere are of major scientific interest. The atmospheric science community is concerned with potential impacts on atmospheric chemistry (including stratospheric ozone) and climate, and uses large eruptions to test climate and global circulation models. Large eruptions are of great interest to volcanologists as they provide insight into the volcanic processes and hazards associated with these rare, high-magnitude events and their frequency on geological timescales. The eruption of the submarine Hunga volcano (Kingdom of Tonga) on 15 January 2022 was among the largest eruptions of any type of the past century, and the largest known historical submarine explosive eruption. The Hunga eruption was similar in magnitude (erupted volume) to the 1991 Pinatubo eruption (Philippines), but distinct in terms of emissions and impacts because Hunga is a submarine volcano, yielding emissions dominated by evaporated seawater and including exotic particles such as sea salts (Chapters 2, 3). This has important implications for the atmospheric and climate impacts of submarine eruptions (Chapters 4, 5, 7). Hunga produced the most energetic volcanic explosion recorded on Earth since the 1883 Krakatau eruption (Indonesia), injecting a volcanic plume into the lower mesosphere (Chapter 6), and the 2022 paroxysm may represent the first example of a well-observed phreatoplinian style eruption. It produced the third-largest stratospheric aerosol perturbation observed in the satellite era (since 1978), after the 1991 Pinatubo and 1982 El Chichón eruptions (Chapter 3).

Chapter 1 provides the volcanological context of the 2022 Hunga eruption. It includes a brief review of explosive submarine volcanism (Section 1.1), some background on Hunga volcano and its tectonic setting in the Tonga-Kermadec volcanic arc (Section 1.1.3), a summary of the main characteristics of the 2022 eruption (sequence of events, eruption magnitude, and potential analogs; Sections 1.2–1.3), and describes the state of the stratosphere prior to the 2022 eruption (Section 1.3). Chapter 2 provides a more detailed account of satellite observations of the 2022 eruption products and the first month of atmospheric residence; this chapter focuses on the volcanological aspects. Chapters 3–7 focus on the later evolution of the stratospheric perturbation by the Hunga eruption and its impacts on atmospheric circulation, chemistry, and climate.

1.1 Introduction to submarine volcanism and Hunga volcano

1.1.1 Submarine volcanism and submarine eruptions

Volcanism on Earth is broadly categorised as either subaerial or subaqueous, according to the realm in which it occurs. Subaqueous volcanism includes any volcanic activity beneath surface water – i.e., the oceans, lakes, and glaciers – and is dominated by submarine volcanism beneath the ocean surface. Subaerial volcanism occurs above the surface of any water body and vents material directly into the atmosphere. Based on total erupted volume, it has been estimated that 85% of volcanism on Earth is subaqueous (~3.5 km^3 erupted magma per year; White et al., 2015). This is due to the prevalence of submarine, mid-oceanic ridge (MOR) spreading centres (which contribute at least ~3 km^3 erupted magma per year), where the majority of Earth's volcanic output occurs (e.g., Deligne and Sigurdsson, 2015). Other submarine volcanism occurs at oceanic islands (or hot spots; e.g., Hawai'i, USA) and in volcanic arcs (e.g., the Tofua arc, Tonga). Volcanic arcs form above subduction zones or convergent plate margins and produce arcuate chains of stratovolcanoes or volcanic islands (Deligne and Sigurdsson, 2015). Although submarine arc volcanism is relatively minor in volumetric terms, it is distinct from the majority of other (mostly effusive) submarine volcanism due to the potential for explosive eruptions and impacts on the atmosphere and climate. Regardless of tectonic setting, the vast majority of submarine volcanic activity is very poorly observed relative to subaerial volcanism due to the challenges of instrumenting and mapping the seafloor, directly observing eruptions beneath the ocean, and accessing submarine volcanic deposits (Abbott and Rubenstone, 2024; Carey et al., 2018). Our limited knowledge of submarine volcanism was highlighted in a National Academies report (NASEM, 2017).

Our understanding of the physical processes controlling the dynamics, style, intensity, and impacts of explosive volcanic eruptions is largely derived from observations of high-magnitude subaerial eruptions in the post-1979 satellite era (e.g., 1980 Mt St Helens, 1982 El Chichón, 1991 Mt Pinatubo) and from analysis of well-preserved deposits of older subaerial volcanic eruptions. Explosive volcanic eruptions are driven by the exsolution of dissolved gases (mostly water [H_2O] and carbon dioxide [CO_2]) and subsequent expansion of gas bubbles as magmas decompress towards atmospheric pressure (0.1 MPa), which ultimately leads

to magma fragmentation and atmospheric injection of gases and ash in a volcanic plume. In the submarine realm (including MOR systems, intraplate hotspots/seamounts, oceanic plateaus, and oceanic volcanic arcs), the high hydrostatic pressure (~1 MPa per 100 m of water depth) can suppress explosive volcanism (e.g., Cas and Simmons, 2018) – except within a few hundred meters of the ocean surface. Hence, perhaps as much as 95% of submarine eruptions are effusive (non-explosive), with explosive submarine eruptions (~5% of submarine eruptions; White et al., 2015) commonly thought to be restricted to water depths of less than a few hundred meters. In shallow subaqueous environments the interaction between hot magma (800–1200°C) and external water (<20°C) can be highly explosive, due to instantaneous superheating and explosive boiling and expansion of liquid water in contact with magma (Molten Fuel-Coolant Interaction or MFCI processes; Cas and Simmons, 2018; Zimanowski et al., 2015; Sparks et al., 1997). Volcanic activity involving external water is called 'phreatomagmatic' (also termed hydrovolcanic or hydromagmatic), one key characteristic of which is the generation of fine ash particles (with diameters <1000 μm or 0.1 mm) via MFCI processes that fragment erupting magma more efficiently than magmatic fragmentation (e.g., Zimanowski et al., 2015).

Individual subaerial and subaqueous (phreatomagmatic) eruptions span orders of magnitude of erupted magma volume, mass flow rate, tephra dispersal (determined by plume height), and energy release. Early classification schemes for volcanic eruptions were based on measurements of the area of dispersal (D, km^2) and degree of fragmentation (F, %) of the resulting pyroclastic fall (tephra) deposits (Walker, 1973). The F parameter represents the percentage of tephra particles in the deposit with diameter of <1 mm, and varies from less than 20 for deposits generated by magmatic fragmentation (via exsolution of volcanic gases), to over 80 for phreatomagmatic eruption deposits (fragmented via MFCI processes). Based on their D and F values, Walker (1973) identified three kinds of pyroclastic fall deposit: Hawaiian/Strombolian (magmatic; low D and low F); Surtseyan (phreatomagmatic; low D and high F); and Plinian (magmatic; high D and low/moderate F). The Walker (1973) classification omitted the phreatomagmatic equivalent of a Plinian eruption. However, some tephra deposits were observed to have widespread dispersal (high D), similar to Plinian tephra, but with a much finer grain size (high F). Self and Sparks (1978) argued that such deposits are the phreatomagmatic analog of Plinian deposits and proposed the term 'phreatoplinian'. Well-preserved phreatoplinian deposits are rare, but archetypal examples include the Oruanui Formation, Taupo volcano, New Zealand (produced by the ~26 ka Oruanui eruption of Taupo, the largest known phreatomagmatic eruption) and the 1875 Askja (Iceland) eruption deposit (e.g., Van Eaton et al., 2012; Houghton et al., 2015). The 1875 Askja eruption is often cited as the only phreatoplinian eruption documented by eye-witness records, but the phreatoplinian phase of the eruption was brief (~1 hr) due to a limited supply of external water from ice melt runoff and groundwater (Houghton et al., 2015). Delos Reyes et al. (2018) assert that the January 1911 eruption of Taal volcano (Philippines), which was well observed, should also be classified as phreatoplinian, but this remains contentious. As discussed later, a significant volcanological aspect of the 2022 Hunga eruption is that it likely represents the first phreatoplinian eruption in the modern instrumental era, although it has yet to be officially classified in this category.

In its Volcanoes of the World (VOTW) database, the Smithsonian Institution's Global Volcanism Program (GVP) lists 120 active Holocene submarine volcanoes, of which 80 have reported eruption dates and 40 have erupted since 1978 (Global Volcanism Program, 2024). Although 70% of the Earth is submarine, only 15% of Holocene arc volcanoes in the VOTW database are submarine (Abbott and Rubenstone, 2024). Most historically active submarine volcanoes are located in the following regions: Japan, Taiwan and the Mariana Islands (Izu–Bonin–Mariana arc); Melanesia (Solomon Islands, Vanuatu, Papua New Guinea); the Tonga–Kermadec Islands; and the Mediterranean Sea (Italy, Greece). Several submarine volcanoes (e.g., Hunga, Home Reef and Lateiki in Tonga, Fukutoku-Oka-no-Ba in Japan) have multiple reported eruptions since 1978; these are also among the shallowest and hence more likely to produce plumes that breach the ocean surface. Abbott and Rubenstone (2024) argue that, due to observational challenges, the VOTW database significantly underestimates the actual number of submarine volcanoes, proposing that >32% of Holocene arc volcanoes are submarine.

One of the key observations arising from the 2022 Hunga eruption is the potential for stratospheric hydration by water vapor emitted by submarine volcanic eruptions (Chapters 2, 3). Water is by far the most abundant volcanic gas species in magmas (typically >90 mol%; e.g., Oppenheimer et al., 2014), but

volcanic emissions of water vapor (WV) are very difficult to quantify (e.g., Millán et al., 2022; Sioris et al., 2016; Murcray et al., 1981), and direct observations of volcanic WV emissions are rare, even after major eruptions. There are three potential sources of WV in emissions from explosive volcanic eruptions: degassing of water from the erupting magma (i.e., "volcanic" water), entrainment of tropospheric WV into the volcanic plume (e.g., Glaze et al., 1997), and, in phreatomagmatic eruptions, the incorporation of external water at the vent (e.g., Rowell et al., 2022). The main factor limiting direct stratospheric WV injection by volcanic eruptions is condensation of water (or deposition of ice) in rising volcanic plumes (e.g., Pitari and Mancini, 2002). Prior to the 2022 Hunga eruption, the potential atmospheric and climate impacts of explosive submarine volcanic eruptions and associated WV emissions had received little attention. Cronin (1971) speculated that submarine and phreatomagmatic volcanic eruptions in the 1960s (e.g., Surtsey, Iceland in 1964; Taal, Philippines in 1965) may have been partly responsible for increases in stratospheric WV observed in that decade. Valentine (1993) suggested that phreatoplinian eruptions could theoretically inject large quantities of WV into the stratosphere, along with very fine ash particles. Joshi and Jones (2009) considered the potential effects of stratospheric WV injection by volcanic eruptions in the context of the 1883 Krakatau (Indonesia) eruption. The 1883 Krakatau eruption generated "co-ignimbrite" clouds rising above pyroclastic density currents (PDCs) that partially flowed over open water (Self and Rampino, 1981; Self, 1992), potentially entraining large amounts of WV that could ascend to stratospheric altitudes in the co-ignimbrite plume (Dartevelle et al., 2002). Joshi and Jones (2009) hypothesised that tropospheric warming due to the stratospheric WV injected via this process could partially offset surface cooling induced by sulfate aerosols.

Satellite observations of recent submarine eruptions and modelling of water-rich plumes have suggested limited potential for climate impacts due to the suppression of eruption column height and low SO_2 emissions due to scavenging by seawater (e.g., Rowell et al., 2022). In the era of satellite measurements (since 1978), only ~13 submarine eruptions (not including the 2021–2022 Hunga eruptions) have been sufficiently energetic to generate plumes that breached the ocean surface and produce potentially detectable SO_2 emissions (Carn et al., 2022). The May 2010 eruption of South Sarigan seamount (CNMI), which produced a subaerial eruption column that rose to ~12 km from an eruption vent at ~200 m water depth (Green et al., 2013; Embley et al., 2014), appears to be the deepest submarine eruption to have produced SO_2 emissions detectable from space to date, although the measured SO_2 mass was low (~1 kiloton, kt). Mastin and Witter (2000) list only two other submarine volcanoes reported to have produced surface breaching from depths of >100 m: at Kick'em Jenny (West Indies) in 1939, 1974 and 1988; and Ritter Island (Papua New Guinea) in 1972 and 1974. In these cases, the subaerial eruption columns extended only a few hundred meters above the ocean surface (Mastin and Witter, 2000). The 2012 eruption of Havre Volcano in the Kermadec Arc is the only deep-sea eruption (~900 mbsl vent) known to have produced an atmospheric plume (Jutzeler et al., 2014; Carey et al., 2018). However, it is debated whether the Havre gas jet extended throughout the water column versus generation of the atmospheric plume by clast–water interactions close to the sea surface (Manga et al., 2018; Knafelc et al., 2022). Modelling of condensable submarine volcanic gas jets suggests that surface breaching is possible from vents as deep as 500 m below sea level (Cahalan and Dufek, 2021).

1.1.2 Introduction to the Tonga (Tofua) arc

Hunga volcano (20.553°S, 175.38°W) is located in the ~800 km-long Tofua volcanic arc, at the northern end of the larger Tonga–Kermadec volcanic arc, which extends north-east of New Zealand into the Pacific Ocean (Figure 1.1). The Tonga–Kermadec arc is the result of westward subduction of the Pacific Plate beneath the Indo-Australian Plate and is one of the most volcanically active island arcs on Earth. Even so, records of volcanic activity are incomplete because most volcanoes in the region are fully or partially submerged, remote, and poorly monitored; hence many eruptions likely go undetected (Yeo et al., 2024). Hunga is one of 14 Holocene volcanoes in the Tofua arc, of which nine are submarine and seven (including Hunga) have been active since 1960 (Global Volcanism Program, 2024). Characterisation of eruption size in the region is challenging, but it is thought that most historic eruptions in the Tofua arc have been relatively small: of the 65 eruptions recorded in the region before 2021, 64 had a Volcanic Explosivity Index (VEI; Newhall and Self, 1982) of 3 or less (Global Volcanism Program, 2024). Prior to the 2022 Hunga eruption, the largest known historic eruption in the Tofua arc was a VEI 4 eruption of Fonualei (Tonga) in

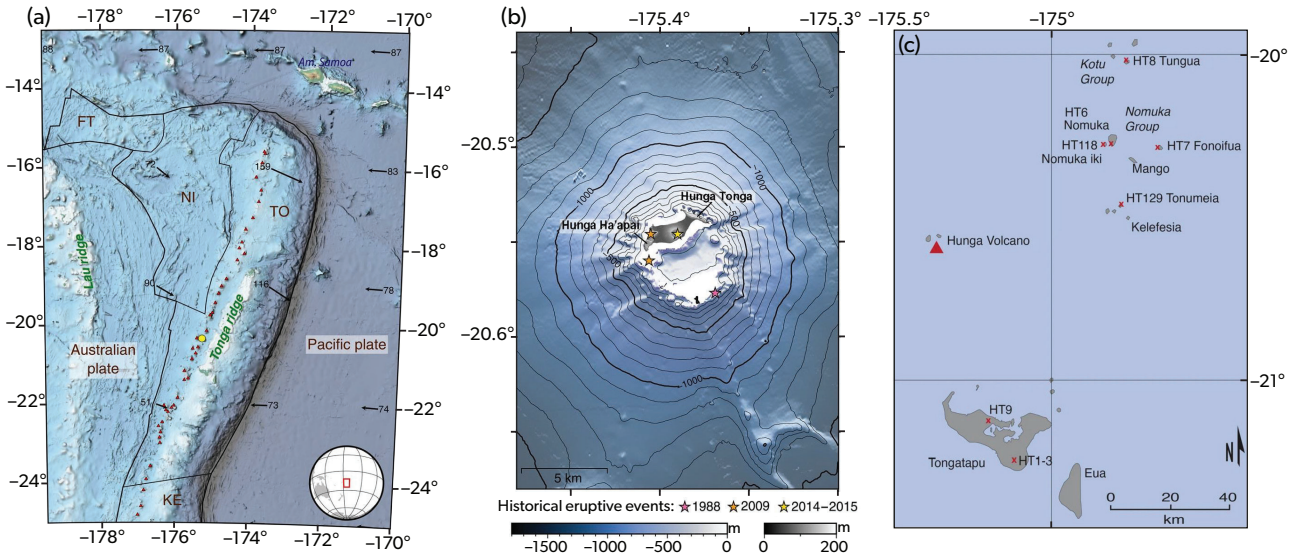

Figure 1.1: *Location map of the Tonga-Kermadec arc and Hunga volcano. (a) Tectonic setting of the Tofua volcanic arc (~21.5°S to 15.5°S), in the northern Tonga-Kermadec subduction zone. The map shows known volcanoes (*red triangles*; includes volcanoes with Holocene eruptions and older volcanoes with no eruptive history), Hunga volcano (*yellow circle*), tectonic plate boundaries (*black lines*), and plate velocities relative to the Australian plate (*black arrows, millimeters per year*). FT, Futuna; NI, Niuafo'ou; TO, Tonga; KE, Kermadec microplates. (b) Pre-2022 multibeam bathymetry of Hunga volcano and topography of Hunga-Tonga and Hunga-Ha'apai islands in September 2017. (c) Location of Hunga (*red triangle*) in relation to other Tongan islands.* Red crosses *show tephra sampling locations after the 15 January 2022 Hunga eruption. Figure taken from Le Mével et al. (2023) and Colombier et al. (2023).*

1846 (although the magnitude is uncertain). Although major explosive eruptions are largely absent from the recent eruptive record, at least eight Tofua arc volcanoes mapped or partially mapped to date have wide (>1 km diameter), flat-bottomed central craters that may be interpreted as calderas produced by large volume, prehistoric eruptions (Yeo et al., 2024). All of them have shallow vents, where the overlying water column would be unlikely to suppress a future explosive eruption, and four of these caldera systems appear to erupt regularly (Curacoa, Volcano-F, Tofua and Hunga), although the 2022 Hunga eruption is the only 'caldera-forming' event in historic times (Yeo et al., 2024). More seafloor surveys, high-resolution bathymetry, seismic surveys, and sediment coring are needed to further characterise the morphology and eruptive history of submarine volcanoes in the Tofua arc.

Due to its oceanic setting, explosive volcanic eruptions in the Tofua arc have the potential to generate a range of volcanic hazards, including:

I. tsunamis (Carvajal et al., 2022; Lynett et al., 2022; Borrero et al., 2023);
II. pyroclastic density currents that travel over the ocean surface (Carey et al., 1996);
III. submarine volcaniclastic density currents (Seabrook et al., 2023; Clare et al., 2023);
IV. pumice rafts (Bryan et al., 2004; Jutzeler et al., 2014; Brandl et al., 2020).

1.1.3 Physical description of Hunga volcano

Hunga volcano is a massive, almost entirely submerged andesitic stratovolcano that rises more than 2 km from the surrounding seafloor, breaching the ocean surface to form the islands of Hunga-Tonga and Hunga-Ha'apai (HTHH; Cronin et al., 2017, Figure 1.1). The latter are the emergent remnants of the rim of a submarine caldera ~6 km in diameter, which formed during a caldera-forming eruption dated to 1040–1180 CE (Cronin et al., 2017; Brenna et al., 2022). Prior to the 2022 Hunga eruption, the caldera depression was up to ~150 meters deep (Figure 1.1), and ignimbrite units emplaced by the 1040–1180 CE caldera-forming eruption formed the topmost deposits on HTHH. At least two additional ignimbrite units and pyroclastic flow deposits preserved on HTHH (as yet undated) are evidence of other, high-magnitude eruptions of Hunga prior to 1040–1180 CE (Cronin et al., 2017; Brenna et al., 2022). The 1040–1180 CE Hunga caldera- forming event has been tentatively proposed (within error bounds) as the source of an unknown

tropical eruption in 1108 CE that produced a sulfate anomaly in ice cores and significant (>1°C) global cooling (Cronin et al., 2017; Sigl et al., 2015).

1.1.4 Historic activity of Hunga volcano

Hunga volcano was relatively active in the century prior to the 2022 eruption, with 5 confirmed eruptions. This contrasts with volcanoes that have produced major (VEI 5+), climate-forcing subaerial eruptions, which typically show centuries of pre-eruptive quiescence (e.g., Pinatubo, El Chichón). Activity at Hunga was first recorded in 1912, but little is known about its earlier eruptive history (Cronin et al., 2017). Shallow submarine eruptions were observed in 1912 (VEI 2), 1937 (VEI 2), and 1988 (VEI 0). These eruptions were all located near a group of shallow reefs about 3 km south of Hunga-Tonga island, on the SE rim of Hunga caldera (Global Volcanism Program, 2022b). Monitoring of more recent eruptions from this remote, largely submarine volcano has benefited from the availability of satellite remote sensing and hydroacoustic monitoring (e.g., Vaughan and Webley, 2010; Bohnenstiehl et al., 2013; Garvin et al., 2018). An eruption in March 2009 (VEI 2) began as a submarine event, progressing to a subaerial eruption as tephra deposits enlarged Hunga-Ha'apai island, although these deposits eroded away within ~6 months (Global Volcanism Program, 2009; Vaughan and Webley, 2010; Bohnenstiehl et al., 2013). Surtseyan eruptions in December 2014 – January 2015 (VEI 2) were also initially submarine prior to subaerial tephra deposition that formed a subaerial tombolo between the two islands of HTHH (Cronin et al., 2017; Garvin et al., 2018; Colombier et al., 2018); this tombolo persisted until the 2022 eruptions (Figure 1.2). After the 2014–15 eruption ended in January 2015, no further activity was reported at Hunga until December 2021 (Global Volcanism Program, 2022b).

1.2 The 2022 Hunga eruption

1.2.1 Short-term precursors to the 2022 Hunga eruption

High-magnitude (VEI 5+) eruptions are often preceded by weeks to months of precursory activity prior to the paroxysmal event (e.g., 1980 Mount St Helens, 1991 Pinatubo), and the 2022 Hunga eruption also followed this pattern. The 2021–2022 Hunga eruptive episode began around 09:35 local time on 20 December 2021 (20:35 UTC on 19 December 2021) with the generation of a ~16–20 km tall plume and a circular umbrella cloud (a density-driven, horizontal intrusion) with a maximum radius of ~130 km from a vent adjacent to the 2014–2015 eruption vent on HTHH (Figure 1.2c; Prata et al., 2025; Gupta et al., 2022; Global Volcanism Program, 2022b). The umbrella cloud persisted for ~5–6 hours (Prata et al., 2025; Gupta et al., 2022). The 19 December 2021 eruption plume was water-ice rich, contained ~10 kt of SO_2, and dusted islands in the Kingdom of Tonga with ash (Gupta et al., 2022; Carn et al., 2022). Although the location of the 19 December 2021 eruption vent (orange line in Figure 1.2c) is subaerial in prior satellite observations on 10 December 2021, it is likely that seawater gained access to the vent early in the eruption to produce the observed water-ice rich plume, with subsequent tephra deposition during the eruption then enlarging the island (Figure 1.2c,d). Following the 19 December 2021 eruption, Surtseyan-style explosions, the creation of steam-rich plumes rising several kilometres, and horizontal steam bursts continued throughout late December 2021 and early January 2022 (Global Volcanism Program, 2022b). These intermittent eruptions also released daily plumes containing up to 15 kilotons of SO_2 (Carn et al., 2022). Occasional strands of floating pumice were found within several kilometres of Hunga in late December 2021, and some drifted to beaches in the Kingdom of Tonga (Global Volcanism Program, 2022b). During this period, HTHH island increased in size from 2 km^2 on 10 December 2021 to 3.6 km^2 on 2 January 2022 by expanding its tephra apron (Global Volcanism Program, 2022b); Figure 1.2d). Several additional small plumes were observed between 1 and 13 January 2022 (e.g., Carn et al., 2022; Gupta et al., 2022).

A major eruptive event occurred on 13 January 2022 at ~15:20 UTC, generating a plume that rose to an altitude of 18–19 km (just above the tropopause at ~18 km) and a 250-km wide ice-rich umbrella cloud containing 60 kt of SO_2 (Prata et al., 2025; Carn et al., 2022; Gupta et al., 2022; Global Volcanism Program, 2022a). The plume was sustained for almost a full day (~22 hours), making this the longest-duration eruptive event of the entire 2021–2022 eruption sequence (Gupta et al., 2022). Ground-based images from the Tonga Geological Survey show Surtseyan-style pulses ejecting dark volcaniclastic material into the air and pyroclastic currents extending into the ocean (Global Volcanism Program, 2022a). Minor ashfall was detected in the Kingdom of Tonga and the Tonga Meteorological Survey issued tsunami warnings from this event (Global Volcanism Program, 2022b). The central section of HTHH island was destroyed by this event, such that the vent from which the eruption had oc-

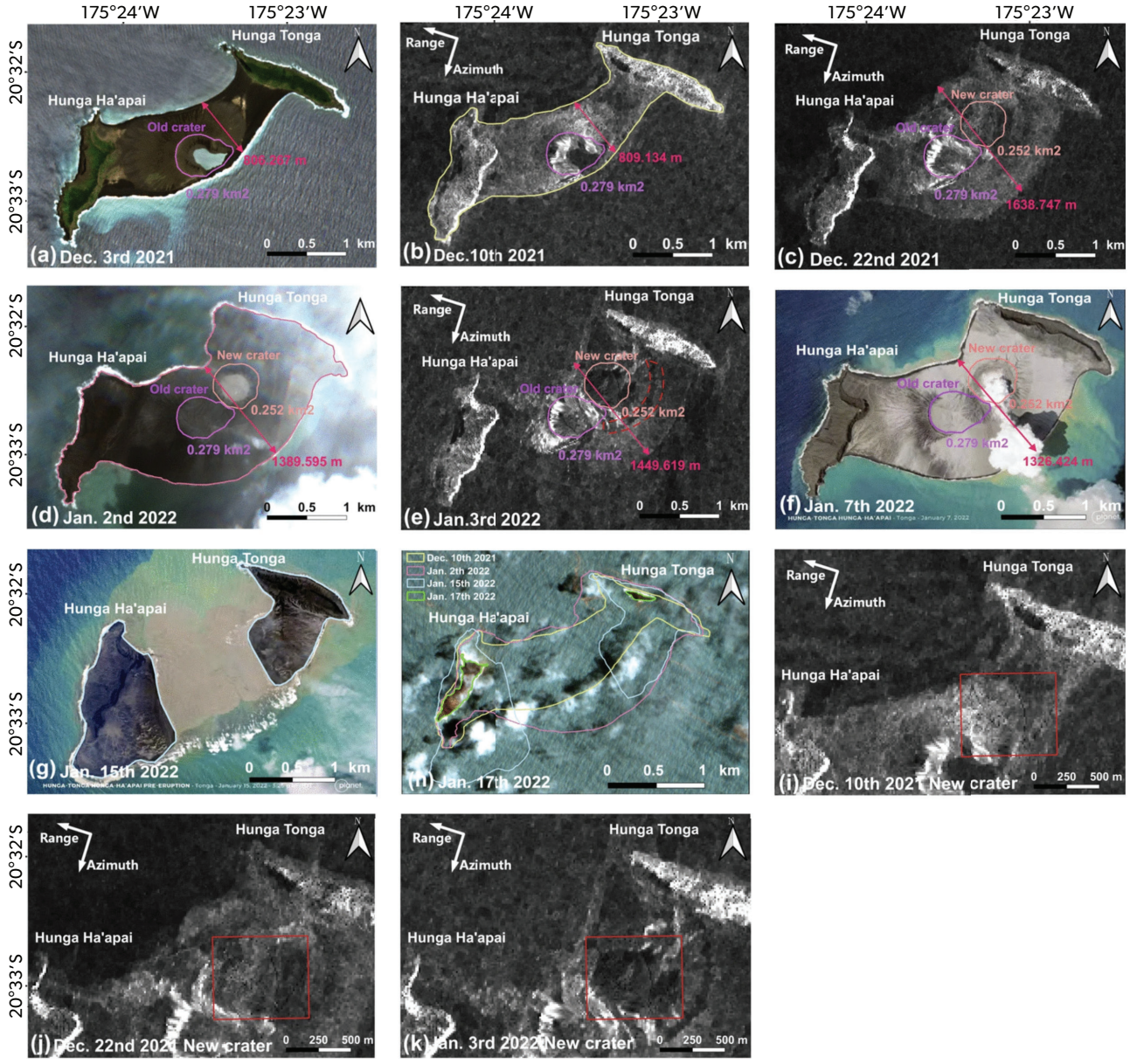

Figure 1.2: *Satellite imagery showing the changing morphology of Hunga-Tonga and Hunga-Ha'apai (HTHH) islands during the 2021-2022 Hunga eruption sequence from December 2021 to January 2022. (a, d, h) Sentinel-2A visible imagery; (b, c, e) Amplitude imagery from the Sentinel-1A radar satellite; (f, g) Planet Labs SkySat imagery (Image © 2022 Planet Labs PBC); (i, j, k) Enlarged regions of Sentinel-1A images on 10 December 2021 (b), 22 December 2021 (c), and 3 January 2022 (e), respectively. Figure taken from Wei et al. (2025).*

curred up to this point was fully submerged below sea level by 15 January 2022 (Figure 1.2).

1.2.2 Description and timeline of the 15 January 2022 Hunga eruption

Following the 13–14 January 2022 eruption, Hunga emitted several short-lived plumes (or puffs) that were visible in satellite imagery rising to the mid- to upper troposphere (Carn et al., 2022; Van Eaton et al., 2023). These plumes contributed negligible mass flux relative to subsequent events, but indicate that the volcanic system remained open immediately prior to the climactic eruption. An eruption start time of ~04:00 UTC (~17:00 local time) on 15 January 2022 is often reported in the literature (Gupta et al., 2022; Matoza et al., 2022) and reflects the sudden onset of plume development (Figures 1.3 and 1.4), audible explosions on Tongatapu (Purkis et al., 2023), geophysical signals such as long-range infrasound (Vergoz et al., 2022; Matoza et al., 2022), and the highest flux phase of the eruption (Gupta et al., 2022; Van Eaton et al., 2023). Loud explosions were heard on Tongatapu at 04:06 and 04:18 UTC, and tsunami waves reached the port of Nuku'alofa (Tongatapu) by 04:26 UTC (Purkis et al., 2023). The timing of these explosions precisely matches explosion onset times estimated from disturbances in ionospheric total electron content, with the strongest explosion occurring at 04:18 UTC (Astafyeva et al., 2022). By 04:36 UTC, the eruption column reached its maximum overshoot height of 57–58 km, in the lower mesosphere (Figure 1.3; Proud et al., 2022; Carr et al., 2022). The umbrella cloud expanded to a diameter of 400 km over the next ~1 hour, coincident with observations of the most intense lightning rates ever documented in Earth's atmosphere (>2,615 flashes min^{-1} at peak intensity (Figure 1.3; Van Eaton et al., 2023). Lateral spread of the volcanic column occurred at two altitudes: 30–40 km for the upper umbrella and 17–20 km (coincident with the tropopause) for the lower umbrella (Figure 1.3; Carr et al., 2022; Gupta et al., 2022). Lapilli (tephra particles with diameters of 2–64 mm) began falling on Tongatapu by ~04:50 UTC, followed by ash (tephra particles with diameters of <2 mm) at ~05:00 UTC (Wu et al., 2025). A blast at 04:56 UTC broke windows in Nuku'alofa, and the largest tsunami reached the port at 05:15 UTC (Figure 1.3; Purkis et al., 2023). Over the next hours the altitude of the upper umbrella cloud declined as the cloud was blown westward by stratospheric winds (Figure 1.3). A brief eruptive pulse occurred close to 08:30 UTC which produced infrasound signals, an overshooting top to 39 km, and renewed lightning (Figure 1.3; Matoza et al., 2022; Gupta et al., 2022; Van Eaton et al., 2023). The umbrella clouds from the Hunga eruption spread over the Kingdom of Tonga (Figures 1.3 and 1.4) and ash fallout produced deposits up to 3.5 cm thick (Figure 1.5; Kelly et al., 2024). Plume heights and volcanic lightning subsided by 15:12 UTC, indicating an end to the eruption (Figure 1.3; Van Eaton et al., 2023).

The impacts of the 15 January 2022 Hunga eruption in the ocean and on the seafloor were significant and widespread. Local tsunamis produced by the 15 January 2022 eruption reached Tongatapu, the largest island in the Kingdom of Tonga, with wave heights over 6 meters (Borrero et al., 2023; Purkis et al., 2023). Photographs taken from a vessel tens of kilometres from Hunga show evidence for a partially collapsing eruption column producing pyroclastic currents that entered the sea (Clare et al., 2023, Figure 1.4). Tonga's domestic and international seafloor communication cables stopped working at 04:30 and 05:44 UTC, indicating the timing of major seafloor disturbances 16–18 km and 47–70 km from the vent, respectively (Figure 1.3; Clare et al., 2023). Comparisons of bathymetry before and after the 2022 eruption revealed that Hunga's caldera floor dropped by ~800 m (Figure 1.6), up to 30 m of scour occurred along the caldera rim, and deposits up to 40 m thick were present outside of the caldera (Seabrook et al., 2023). Together, the bathymetry changes and the timing of cable breakage have been interpreted to indicate that the 15 January eruption produced fast-moving volcaniclastic density currents along the seafloor (Seabrook et al., 2023; Clare et al., 2023). Serendipitous remotely operated vehicle (ROV) dives in the Lau Basin in March/April 2022 demonstrate that Hunga's submarine volcaniclastic currents travelled at least 80 km west of the vent and buried benthic communities as they travelled (Beinart et al., 2024; Seabrook et al., 2023; Chaknova et al., 2025).

The 15 January 2022 Hunga eruption was highly explosive, and certainly driven at least in part by phreatomagmatic processes. It is likely to meet the criteria for a phreatoplinian eruption (e.g., wide dispersal of fine ash; pulsating eruption column behavior; Van Eaton et al., 2012), in which case it would be the first such event in the modern era. However, work is ongoing to fully characterise the products of the 2022 eruption and elucidate the role of external water versus internal magmatic processes in triggering the event.

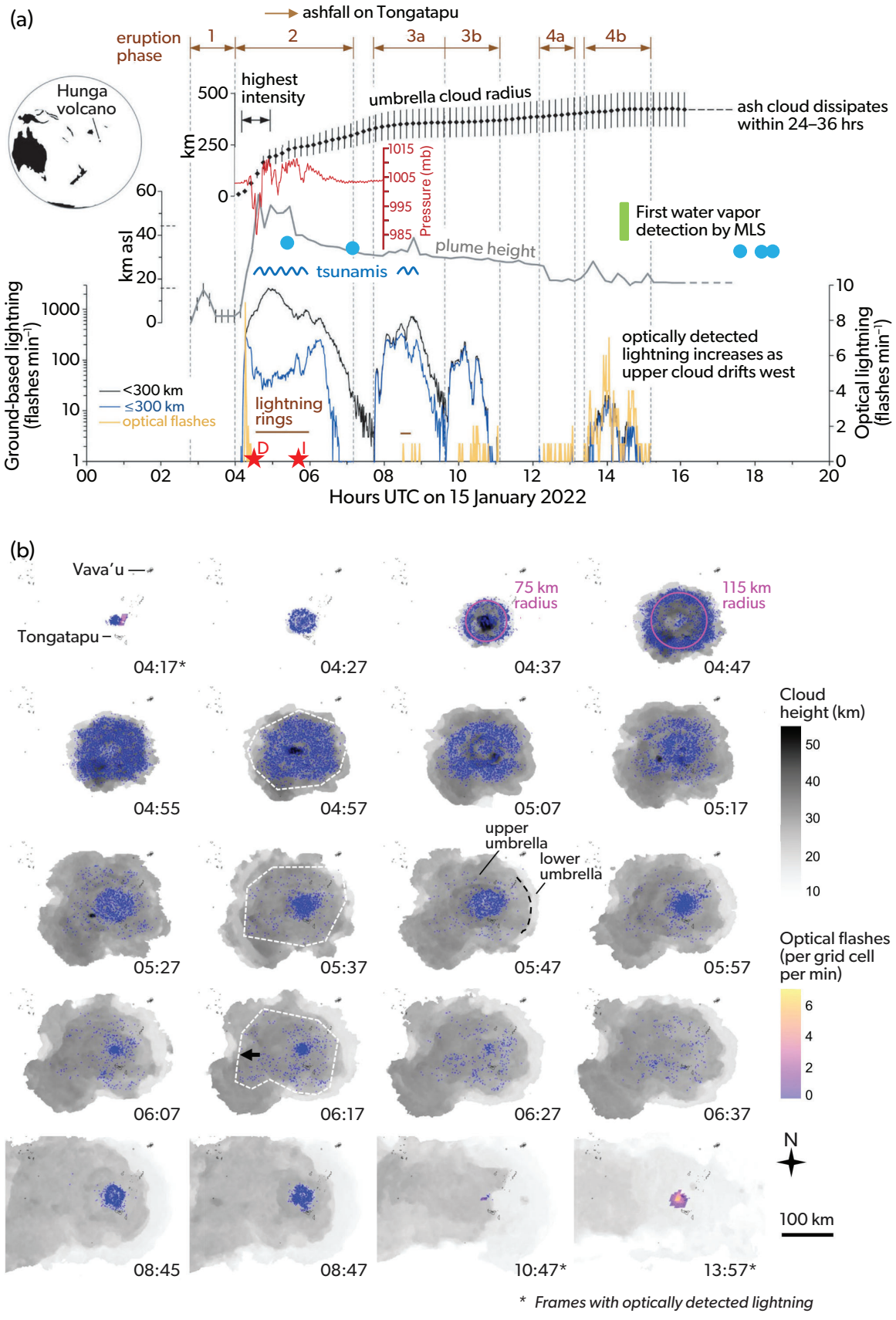
(a)
ashfall on Tongatapu
eruption phase
1
2
3a
3b
4a
4b
Hunga volcano
highest intensity
umbrella cloud radius
ash cloud dissipates within 24–36 hrs
km
500
250
0
1015
1005
995
985
Pressure (mb)
First water vapor detection by MLS
km asl
60
40
20
0
plume height
tsunamis
optically detected lightning increases as upper cloud drifts west
Ground-based lightning (flashes min⁻¹)
1000
100
10
1
<300 km
≤300 km
optical flashes
lightning rings
D
I
Optical lightning (flashes min⁻¹)
10
8
6
4
2
0
00
02
04
06
08
10
12
14
16
18
20
Hours UTC on 15 January 2022
(b)
Vava'u
Tongatapu
75 km radius
115 km radius
04:17*
04:27
04:37
04:47
04:55
04:57
05:07
05:17
upper umbrella
lower umbrella
05:27
05:37
05:47
05:57
06:07
06:17
06:27
06:37
08:45
08:47
10:47*
13:57*
Cloud height (km)
50
40
30
20
10
Optical flashes (per grid cell per min)
6
4
2
0
N
100 km
* Frames with optically detected lightning

Figure 1.3: *(a) Satellite, volcanic lightning and surface pressure chronology of the 15 January 2022 Hunga eruption. Four phases of eruptive activity can be distinguished using umbrella cloud growth, maximum plume heights over Hunga volcano, and lightning rates (with phases 3 and 4 subdivided based on variable lightning rates). Lightning detected by ground-based networks is shown on the left axis (log scale) in terms of flashes* min^{-1} *occurring within 300 km (*black line*) and 20 km of Hunga (*blue line*). Optically detected flash rates from the GOES-17 satellite (*yellow bars*) are shown on the right axis (linear scale) and include lightning detected within 250 km of the volcano. The timing of lightning rings described by Van Eaton et al. (2023) is indicated by two horizontal lines. Heights of the tropopause (~17 km) and stratopause (~43 km) are shown as dashed lines on the plume height axis, given in km above sea level (asl).* Red line *shows barometric pressure (millibars, mb) recorded at Nuku'alofa (Tongatapu) from 04:00-08:00 UTC (Purkis et al., 2023), with pressure drops indicating major explosions at Hunga.* Blue wave *indicates the timing of tsunamis on Tongatapu (Purkis et al., 2023; Wu et al., 2025).* Green bar *indicates the timing (~14:30 UTC) and vertical extent (~38–54 km) of the first Hunga water vapor detection by the Aura/Microwave Limb Sounder (MLS).* Blue circles *indicate Hunga plume heights determined from Constellation Observing System for Meteorology, Ionosphere, and Climate (COSMIC)-2 radio occultation (RO) measurements, which are sensitive to atmospheric moisture (Babu and Lin, 2023).* Red stars *on the time axis indicate the inferred times that the domestic (D) and international (I) seafloor telecommunications cables in Tonga were broken by submarine volcaniclastic density currents (Clare et al., 2023); (b) Satellite observations of volcanic plume and lightning development during the 15 January 2022 Hunga eruption, with times shown in UTC.* Grayscale *gives stereoscopic cloud heights derived from geostationary satellite imagery (NOAA/GOES-17 and JMA/Himawari-8),* blue dots *show lightning flashes detected by ground-based radio frequency networks over the following minute, and* purple-yellow color scale *shows optically detected lightning from the Geostationary Lightning Mapper (GLM) sensor on GOES-17. (*) indicates frames with optically detected lightning.* Pink circles *outline a distinctive lightning ring in two frames, showing an (average) expansion rate exceeding 60 m* s^{-1}*. Westward advection of the upper umbrella cloud starts to reveal a lower level cloud by 05:37 UTC.* White dashed polygons *outline the lightning locations, showing their westward movement with the stratospheric umbrella cloud. Local islands are outlined in black. Figure modified from Van Eaton et al. (2023).*

Analysis of gravity data derived from satellite altimetry before and after the 2022 eruption suggests that the Hunga magmatic system consisted of multiple magmatic reservoirs that were tapped and reorganised during the 2021–2022 events, and that eruptible magma remains below Hunga post-2022 (Le Mével et al., 2023). International research cruises are planned in the coming years to further map and sample the extensive submarine deposits from the 2022 Hunga eruption, in order to elucidate the dominant volcanic processes during the eruption and refine estimates of eruption magnitude (Section 1.2.3).

1.2.3 Eruption magnitude assessment

Assessment of the size or magnitude of a volcanic eruption is a critical step that permits comparison with other historic and prehistoric events and analysis of the relationship between eruption magnitude and frequency on various timescales. Two quantities that are commonly used to define the scale of an eruption are magnitude (the total mass or volume of material erupted) and intensity (the mass eruption rate, MER [kg s^{-1}]), both of which can be estimated for modern and ancient eruptions (Pyle, 2015). The most widely used eruption magnitude scale is the VEI, which is an integer scale from 0 to 8 that is assigned based on the erupted volume of juvenile material (tephra) or the eruption column height (Newhall and Self, 1982). Measurement of erupted mass or volume (e.g., based on mapping of deposits in the field or inferred from caldera volume) provides the most robust indication of VEI and is the technique primarily used to assign VEIs to eruptions prior to the era of satellite observations. For modern eruptions, a common approach is to use a well-established relationship between eruption column height in the atmosphere and intensity or MER (Mastin et al., 2009); satellite observations of column height are integrated over the duration of an eruption to estimate the total erupted mass. Due to the complexities of magma–water interaction, which can modify eruption dynamics and plume rise heights (Mastin et al., 2024; Rowell et al., 2022), it can be challenging to rely solely on atmospheric column height to estimate the VEI of submarine eruptions. One limitation of the VEI scale is that it is discrete; continuous scales of magnitude and intensity have been defined based on the logarithm of erupted mass and mass eruption rate, respectively (Pyle, 2015). For reference, the 1991 Pinatubo eruption erupted a total bulk volume of 8.4–10.4 km^3 (3.7–5.3 km^3 dense rock equivalent, DRE), resulting in a VEI of 6 and a magnitude of 6.1.

Assessment of magnitude for submarine volcanic eruptions is inherently more challenging than for

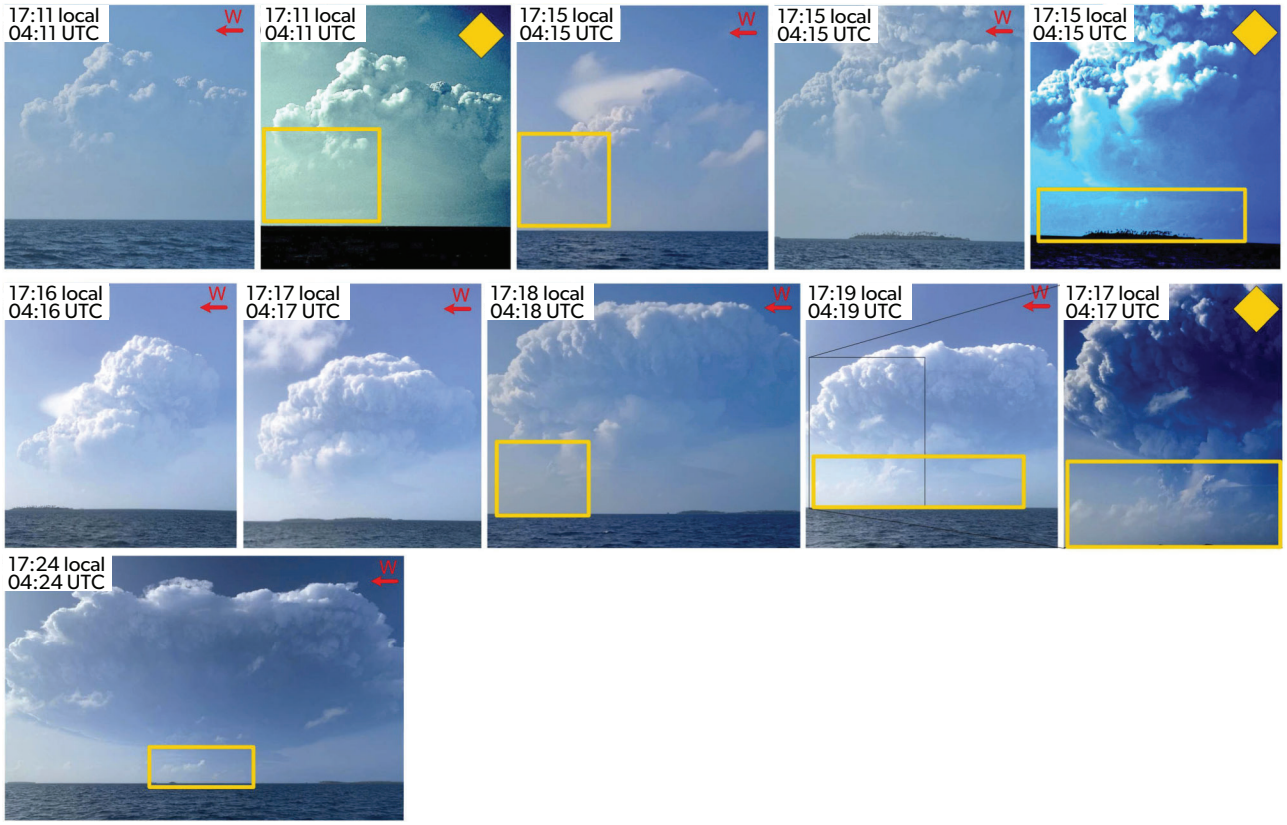

Figure 1.4: *Photographs of the 15 January 2022 Hunga eruption plume (taken by Branko Sugar, South Sea Charters, Nuku'alofa, using a mobile phone). Images marked with a yellow diamond have had contrast or colors enhanced to clarify features in the eruption plume. Red arrows point westward. Images at 04:11 UTC show the initial explosive event and the possible onset of column collapse on the western side of the plume (*yellow boxes*). After the larger explosion at 04:15 UTC the eruption column grows substantially, with skirt clouds at the base of the column indicating column collapse from the plume margins into the ocean and/or steam clouds rising from submarine pyroclastic flows (*yellow boxes*). Similar skirt clouds are also observed in images taken at 04:18, 04:19 and 04:24 UTC. Figure taken from Clare et al. (2023).*

subaerial eruptions. This is due to the difficulty of quantifying the mass or volume of erupted material emplaced underwater and the volume of ashfall deposited over the open ocean. Initial estimates of the magnitude of the Hunga eruption were thus based on satellite observations of eruption column height and inferred from the seismic energy released by the paroxysmal explosions (Table 1.1). Although the 2021–2022 Hunga eruptions comprised several discrete explosive events (19 December 2021, 13–14 January 2022, and 15 January 2022), the eruption magnitude is assigned based on the paroxysmal event that began at 04:14:45 UTC on 15 January 2022 (Matoza et al., 2022). This event generated both the highest volcanic plume (~57–58 km altitude) and the fastest-growing umbrella cloud (reaching 450 km diameter within 50 min) observed in the satellite era (Figure 1.3; Proud et al., 2022; Mastin et al., 2024; Prata et al., 2025). The maximum Hunga plume height and umbrella cloud growth rate exceeded the climactic 1991 Pinatubo plume by 10–20 km and 60%, respectively (Mastin et al., 2024; Prata et al., 2025). Based on conventional relationships between umbrella-growth rate and MER (which, notably, were not calibrated using any large submarine volcanic eruptions or plume heights over 35–40 km), the estimated paroxysmal Hunga MER was ~5–6 × 10^9 kg s^{-1}, which would theoretically have injected 7.2–8.6 km^3 of tephra (DRE) in 1 hour, exceeding the ~5 km^3 (DRE) erupted by Pinatubo in 1991 (Van Eaton et al., 2023; Mastin et al., 2024). However, mapping of tephra fall deposits on islands in Tonga and analysis of ocean discoloration by ashfall yielded a minimum bulk airfall volume of only 1.8 km^3 (0.36–0.75 km^3 DRE; Figure 1.5; Kelly et al., 2024).

Subsequent bathymetric mapping of Hunga volcano revealed a large crater or caldera-collapse structure ~850 m deep (~700 m deeper than the pre-eruption

Table 1.1: *Estimates of magnitude, energy release and volume for the 2022 Hunga eruption.*

Magnitude/VEI/Energy	Volume (km^3)	Technique	Reference
M_s 5.8		Surface seismic waves	USGS NEIC (real-time)
VEI 6		Seismic explosion impulse	Poli and Shapiro (2022)
M_w 5.7–5.8		Seismic data inversion	International Seismological Centre (2022)
M_w 6.34		Seismic data inversion	Thurin et al. (2022)
10–28 EJ		Surface pressure inversion	Wright et al. (2022)
	10	Submarine deposits (total, bathymetry)	Seabrook et al. (2023)
	6.3	Submarine deposits (uncompacted)	Seabrook et al. (2023)
	6.0	Caldera volume (DRE)	Seabrook et al. (2023)
	3.5	Loss from outer flanks (uncompacted)	Seabrook et al. (2023)
	0.4–0.8	Airfall volume estimate (DRE)	Kelly et al. (2024)
	0.03–0.6	Airfall volume (based on sea salt deposits, DRE)	Colombier et al. (2023)

VEI = volcanic explosivity index; M_s = surface wave magnitude; M_w = moment magnitude; EJ = exajoules (1 EJ = 10^{18} J); DRE = dense rock equivalent.

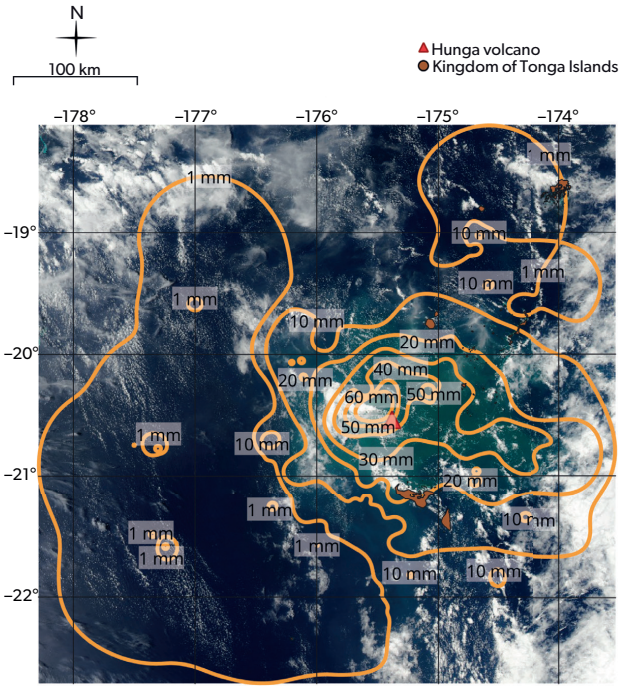

Figure 1.5: *Contour (isopach) map of Hunga ashfall (thickness in millimeters, mm) overlain on a true-color image from NASA's Aqua/Moderate Resolution Imaging Spectroradiometer (MODIS) on 17 January 2022 at 01:42 UTC. Aqua/MODIS image shows ocean discoloration around Hunga volcano (*red triangle*) due to suspended volcanic ash in the water column. Tephra thicknesses are derived from direct measurements on islands, and inferred from MODIS satellite observations of ocean discoloration over the open ocean. Figure from Kelly et al. (2024).*

seafloor), 4 km in diameter and ~6.85 km^3 in volume (Figure 1.6), with 6.3 km^3 of uncompacted deposits emplaced on the volcano's flanks by submarine density currents (Wu et al., 2025; Clare et al., 2023; Seabrook et al., 2023, Table 1.1). Note that it remains uncertain whether the submarine void produced by the eruption is a caldera (implying structural collapse after magma removal) or an explosion crater (excavated by phreatomagmatic activity), or if it was formed by a combination of processes (Walker and de Ronde, 2024). This interpretation also impacts estimates of the relative volume of juvenile (i.e., fresh magma) and pre-existing material discharged by the eruption. Combining the airfall tephra and submarine deposit volumes yields a total bulk erupted volume of ~8 km^3 for the 15 January 2022 Hunga eruption, with most (~75%) of the deposits emplaced by submarine gravity currents. A bulk volume of ~8 km^3 suggests that the 2022 Hunga eruption was a high-end VEI 5 event, as currently listed in (Global Volcanism Program, 2024). Alternatively, assuming that the caldera collapse volume (~6.85 km^3) represents the DRE eruption volume yields a VEI of 6 (Wu et al., 2025). Given the uncertainties on eruption volumes, it is therefore likely that the 2022 Hunga eruption was a similar magnitude to the 1991 Pinatubo eruption (VEI 6), and certainly larger than other VEI 5 eruptions since 1979 (Table 1.2). Estimates of juvenile magma discharge into the atmosphere based on sea salt deposition on tephra (~0.03–0.6 km^3; Colombier et al., 2023) are broadly consistent with the estimated airfall tephra volume (Kelly et al., 2024, Table 1.2).

Seismic energy released by the paroxysmal explosive phase of the 15 January 2022 Hunga eruption was also used to provide rapid (near real-time) estimates of earthquake magnitude, which were an early indic-

Table 1.2: *Major (VEI 5+) volcanic eruptions since 1979.*

Eruption	Date	VEI	Volume (bulk, km^3)	Volume (DRE*, km^3)	Reference
Hunga (Tonga)	Jan 15, 2022	5–6	8	6?	Seabrook et al. (2023)
Cordon Caulle (Chile)	Jun 2011	4–5	2.4	–	Delgado et al. (2019)
Cerro Hudson (Chile)	Aug 1991	5	4.3	2.7	Kratzmann et al. (2009)
Pinatubo (Philippines)	Jun 1991	6	8.4–10.4	3.7–5.3	Scott et al. (1996)
El Chichón (Mexico)	Mar–Apr 1982	5	2.2	1.1	Carey and Sigurdsson (1986)
Mt St Helens (USA)	May 1980	5	1.3	–	Tilling et al. (1990)

*DRE: dense rock equivalent (i.e., void-free).

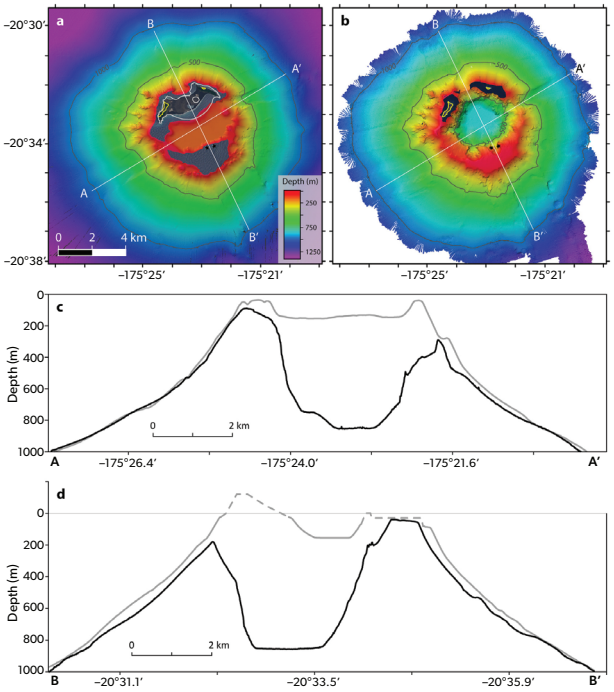

Figure 1.6: *Changes to the seafloor due to the 15 January 2022 Hunga eruption: (a) pre-eruption bathymetry from 2016. White polygon outlines HTHH island in early January 2022, including its crater lake (Figure 1.2d). Depth color scale and scale bar are the same for (b). Transects A-A' and B-B' (*white lines*) show locations of depth profiles shown in (c) and (d), respectively. (b) Post-eruption bathymetry mapped by USV Maxlimer in July/August 2022 (NIWA-Nippon Foundation TESMaP project, 2023) (c) depth profiles along line A-A' from 2016 (gray) and 2022 (black); (d) depth profiles along line B-B' from 2016 (gray, dashed line estimates height of HTHH island built during 2015 eruption and south rim shoal that was too shallow to map in 2016) and 2022 (black). Yellow polygons in (a) and (b) show remaining above-sea-level extent of the HTHH islands, post-eruption. Figure taken from Henley et al. (2024).*

ation of the size of the event (Table 1.1). Although earthquake magnitudes are not appropriate for scaling volcanic eruptions (Ringler et al., 2023), Poli and Shapiro (2022) used broadband seismic data to measure the paroxysmal explosion impulse and derive a magnitude of 5.8 (VEI 6) for the Hunga eruption (Table 1.1). Magnitudes derived from seismic data are thus consistent with the VEI derived from measurements of erupted volume.

Although, in volumetric terms, the Hunga eruption was not exceptional relative to other major volcanic eruptions of recent decades, it is the size of the paroxysmal explosion on 15 January 2022 that sets it apart from other events in the modern geophysical record. Wright et al. (2022) estimated a single-event energy release from the initial explosion on 15 January 2022 of 10–28 exajoules (EJ; 1 EJ = 10^{18} J), likely larger than the 1991 Pinatubo eruption (~10 EJ), and possibly comparable to the 27 August 1883 Krakatau explosion (~30 EJ). The 2022 Hunga eruption generated a broad range of atmospheric waves, including external Lamb waves, acoustic waves and internal gravity waves (see Chapter 6). The 1883 Krakatau and 1991 Pinatubo eruptions also produced strong Lamb waves visible in surface pressure observations. Global propagation of infrasound and Lamb waves were also reported for VEI ≥ 5 eruptions at Bezymianny (Russia) in 1956, Mt. St. Helens (USA) in 1980, and El Chichón (Mexico) in 1982 (Vergoz et al., 2022). The surface-guided Lamb wave generated by the 15 January 2022 Hunga eruption was observed propagating for four passages around the Earth over six days, approximately the same as observed for the 1883 Krakatau eruption (Matoza et al., 2022). The atmospheric pressure pulse generated by the Hunga eruption was found to be comparable to that of the 1883 Krakatau eruption, although the Krakatau pulse was approximately 30% longer in duration at comparable stations (Matoza et al., 2022). Accounts of audible sound were reported at distances of up to ~17,000 km from Hunga (Matoza et al., 2022; Kraft et al., 2023), compared to ~4,800 km for Krakatau in 1883.

The driving mechanism responsible for the par-

oxysmal Hunga explosion and exceptional plume height remains a subject of debate. Mastin et al. (2024) propose that steam (i.e., evaporated seawater) rising from intense phreatomagmatic jets and/or submarine pyroclastic density currents was the principal source of heat that boosted the height of the Hunga eruption plume (as opposed to hot tephra that supplies heat in subaerial eruptions). Such a process would be consistent with the relatively modest tephra-fall deposits, and with the presence of high concentrations of sea salts in Hunga tephra collected shortly after deposition, which is attributed to significant seawater evaporation during the eruption (Colombier et al., 2023). It would also provide a mechanism for the stratospheric injection of sea salt (Colombier et al., 2023; Vernier et al., 2025). Henley et al. (2024) invoke a non-phreatomagmatic eruption trigger whereby the eruption was driven by the explosive release of pressurized magmatic gases trapped beneath a sealed carapace. However, this theory is difficult to reconcile with the persistent activity at Hunga in the month prior to the 15 January 2022 eruption, including the large eruption on 13–14 January, which indicate a more open volcanic system.

The Mastin et al. (2024) model requires input of ~2900 Tg of steam during the first hour of the 15 January 2022 eruption to propel the Hunga plume to the observed altitude (Figure 1.3; Wu et al., 2025). Petrological analyses of Hunga tephra suggest that a maximum of 319 Tg of water would have degassed from the magma during the eruption (Figure 1.7; Wu et al., 2025), i.e., an order of magnitude less than the required mass of steam, confirming that evaporated seawater was the dominant source of WV in the Hunga plume. Petrological data also elucidate the sulfur budget of the Hunga eruption (Wu et al., 2025). Measurements of sulfur concentrations in Hunga tephra indicate that the magma degassed up to ~19 Tg of SO_2 during the eruption, but only ~7% of this SO_2 (1.3 Tg) entered the atmosphere, with the rest likely absorbed by the ocean or sequestered on ash deposits (Figure 1.7; Wu et al., 2025). The implication is that, had the 2022 Hunga eruption been subaerial rather than submarine, the stratospheric SO_2 injection might have been comparable to the 1991 Pinatubo eruption.

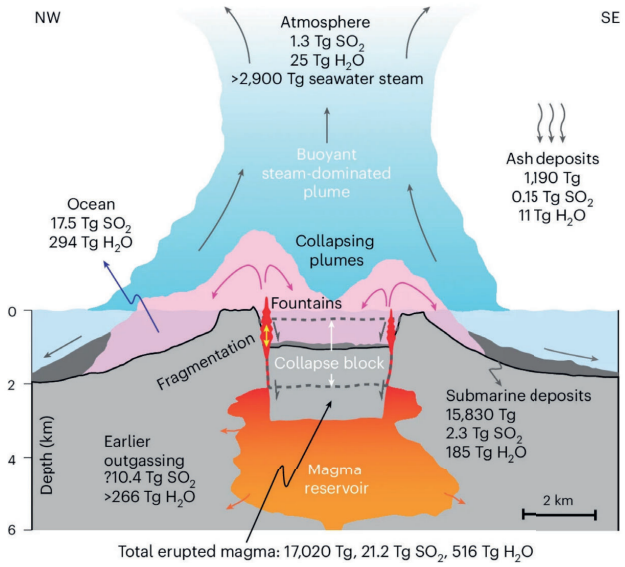

Figure 1.7: *Conceptual model of the 15 January 2022 Hunga eruption showing the initial mass of sulfur dioxide (SO_2) and water (H_2O) in the erupted magma and its final partitioning into pre-eruption outgassing, elements trapped within volcanic deposits, and gas released into the atmosphere and ocean. These values are based on a magma volume of 6.75 km^3 and concentrations of volatiles in the magma preceding the eruption estimated by analysis of melt inclusions. The calculated atmospheric injection of 1.3 Tg SO_2 is close to the upper limit of SO_2 emission estimated from satellite measurements (Carn et al., 2022; Sellitto et al., 2022; Sellitto et al., 2024). Magma fragmentation mainly occurred 400–1,000 m below sea level. The position of the pre-eruption caldera floor is shown by a* dotted line*, with the final position indicating that a 1-km block collapse occurred onto the emptying magma reservoir. Figure from Wu et al. (2025).*

1.2.4 Response to the 2022 Hunga eruption

Rapid responses to collect in-situ observations after major volcanic eruptions enable timely, initial estimates of potential climate impacts and also provide critical opportunities to advance volcano science (NASEM, 2017). NASA has developed a volcanic eruption response plan to maximize the quantity and quality of observations it makes following major eruptions (Carn et al., 2021). Activation of an eruption response is primarily contingent on the magnitude and altitude of volcanic SO_2 emissions measured by satellites. On the basis of prior eruptions, NASA considers that an injection of ~5 teragrams (5 Tg; 5 million metric tons) of SO_2 or more into the stratosphere has sufficient potential for climate forcing of -1 W m^{-2} and warrants the deployment of substantial observational assets, including rapid response balloons and high-altitude aircraft (Carn et al., 2021). Although the 2022 Hunga eruption was undoubtedly a major event, early satellite measurements of SO_2 loading well below the ~5 Tg threshold (~0.5–1 Tg; Carn et al., 2022; Sellitto et al., 2022; Sellitto et al., 2024) suggested that significant climate impacts were unlikely, precluding an imme-

diate NASA response. Additional complications were the exceptional plume height (~30–58 km), which is above the ceiling of high-altitude research aircraft, and the southern hemisphere location of the eruption, limiting available sites for ground-based observations of the Hunga eruption plume.

The principal rapid response to the 2022 Hunga eruption from the atmospheric sciences community involved balloon sonde flights and lidar measurements from the high-altitude Maïdo Atmospheric Observatory on La Réunion (21.1°S, 55.3°E), ~8000 miles west of Tonga (Kloss et al., 2022; Asher et al., 2023; Baron et al., 2023). These observations sampled the stratospheric Hunga SO_2 and aerosol plume as it drifted west from the volcano, 7–10 days after the 15 January 2022 eruption. The U.S. National Oceanic and Atmospheric Administration (NOAA) Earth Radiation Budget program's Baseline Balloon Stratospheric Aerosol Profiles (B^2SAP) project supported the Tonga volcano Rapid Response Experiment (TR^2Ex) on Réunion (Asher et al., 2023), which was coordinated with additional sonde and lidar measurements at the Maïdo Observatory (Kloss et al., 2022; Baron et al., 2023). TR^2Ex deployed a suite of balloon-borne instrumentation to collect high-resolution vertical profiles of SO_2, H_2O and ozone to ~30 km altitude and information on the aerosol size distribution in the plume (Asher et al., 2023). TR^2Ex instruments were unable to measure components of the volcanic plume detected above 30 km by satellite and ground-based remote sensing (Taha et al., 2022; Baron et al., 2023) as these were above the operational ceiling of balloon sondes. Later in 2022, further balloon sonde measurements of the Hunga aerosol plume as it descended in altitude were made from Bauru, Brazil (22.36°S, 49.03°W) during the NASA-supported Brazil Volcano (BraVo) project in May–August 2022 (Souza et al., 2025; Vernier et al., 2025).

The extent of airfall tephra deposits available for direct sampling was limited by land area (Figures 1.1 and 1.5), but concerted efforts were made to sample Hunga tephra as soon as possible after the 15 January 2022 eruption. Samples of Hunga ashfall were collected on islands in Tonga (including Tongatapu and islands E–NE of Hunga; Figure 1.1) between one day and two weeks after the eruption (Wu et al., 2025; Chaknova et al., 2025; Colombier et al., 2023). Airfall tephra thickness and surface density measurements were also made throughout Tonga between a few days and ~5 months after 15 January (Kelly et al., 2024). In April 2022, submarine tephra samples were collected ~100–200 km west of Hunga at depths of ~1.8–2.8 km below sea level in the Lau back-arc basin, using the ROV *Jason* (National Deep Submergence Facility, Woods Hole Oceanographic Institution; Chaknova et al., 2025). Sediment cores containing Hunga tephra were also collected from the flanks of the volcano during phase 1 of the National Institute for Water and Atmospheric Research (NIWA) – Nippon Foundation's Tonga Eruption Seabed Mapping Project (TESMaP-1) in April–May 2022 (Seabrook et al., 2023). Analyses of major elements in subaerial and submarine samples of juvenile Hunga tephra showed consistent silica (SiO_2) contents of 55–60 wt%, corresponding to basaltic andesite or andesite composition (Chaknova et al., 2025; Wu et al., 2025; Seabrook et al., 2023). This is similar to the 2009 and 2014–15 Hunga eruptions, and within the known compositional range of all historic and prehistoric Hunga eruptions and other Tofua arc magmas (~50–62 wt% SiO_2; Brenna et al., 2022). The bulk and skeletal (void-free) densities of airfall tephra were determined to be 1.12 g cm^{-3} and 2.68 g cm^{-3}, respectively (Kelly et al., 2024), the latter consistent with the density of andesite magma. A notable characteristic of all Hunga tephra samples is the dominance of fine and very fine ash particles (<100–300 μm diameter; Chaknova et al., 2025; Wu et al., 2025; Seabrook et al., 2023; Colombier et al., 2023). The predominance of fine ash, coupled with evidence of phreatomagmatic fragmentation (via MFCI) and rapid quenching below sea level (Wu et al., 2025), is indicative of a high-intensity, phreatomagmatic (i.e., phreatoplinian) eruption.

Given the submarine nature of the event, a critical component of the Hunga eruption response involved research cruises to collect bathymetric data and assess impacts to the seafloor and the status of any ongoing submarine volcanic and/or hydrothermal activity (Walker and de Ronde, 2024). Ships equipped for such a response are a limited resource, and rapid response cruises can be difficult to mobilise in remote locations (Walker and de Ronde, 2024). There are also safety concerns for vessels sailing over an active submarine volcano, and response to the Hunga eruption was further complicated by restrictions in place at the time due to the COVID-19 pandemic (Walker and de Ronde, 2024). GNS Science (New Zealand) organised the first post-eruption expedition to collect bathymetric data at Hunga volcano in April 2022 (~2.5 months after the eruption) but was forced to turn back when the multibeam sonar unit was damaged en route (Walker and de Ronde, 2024). In April–May 2022, TESMaP-1

mapped the seafloor surrounding Hunga volcano to a distance of 20 km, and collected sediment cores and seawater samples, but did not sail directly over the 2022 eruption crater due to safety concerns (Seabrook et al., 2023). The first bathymetric map revealing the large ~850 m deep crater structure formed by the Hunga eruption was produced in late May 2022 by a team from the University of Auckland (New Zealand) and Tonga Geological Services (Walker and de Ronde, 2024). In July–August 2022, TESMaP phase 2 (TESMaP-2) utilised the uncrewed surface vessel (USV) Maxlimer (SEA-KIT International) to investigate any ongoing hydrothermal or eruptive activity within the crater and map the bathymetry of the post-eruption edifice at higher spatial resolution (Figure 1.6; Walker and de Ronde, 2024).

1.3 The 2022 Hunga eruption in the context of other historic eruptions

In terms of explosivity, maximum plume height and stratospheric impact (dominated by water vapor injection) there is no analog of the 2022 Hunga eruption in the modern geophysical or instrumental era. As such, it provides the first detailed observational record for a high-intensity, explosive submarine (potentially phreatoplinian) volcanic eruption and greatly improves our understanding of the potential hazards and impacts of these events.

There are other examples of smaller submarine (or partly submarine) eruptions that show some similarities to Hunga. The 1994 eruption of Rabaul (Papua New Guinea; VEI 4) provided the first satellite measurements of an ice-dominated, stratospheric volcanic cloud with modest SO_2 loading (~0.2 Tg), attributed to the entry of seawater into the eruption vent (Rose et al., 1995). Shallow, submarine explosions at Bogoslof volcano (Alaska, USA) in 2016–17 produced ash-poor, water-rich plumes with SO_2 emissions possibly affected by scrubbing of soluble SO_2 by seawater (Lyons et al., 2019; Lopez et al., 2020). In December 2018, phreatomagmatic activity at Anak Krakatau (Indonesia) generated a sustained, lower stratospheric plume that was ice-rich and ash-poor, also with relatively low SO_2 content (~0.06 Tg; Prata et al., 2020). The January 2020 phreatomagmatic eruption of Taal volcano (Philippines) erupted through a pre-existing crater lake and produced a water-rich plume (containing ~0.2 Tg SO_2) and abundant lightning (Van Eaton et al., 2022; Perttu et al., 2023). The August 2021 eruption of Fukutoku-Oka-no-ba (Japan) produced another tephra-poor, water-rich plume from a shallow submarine vent, along with a pumice raft and new islands (~0.02 Tg SO_2; Fauria et al., 2023; Maeno et al., 2022). Despite its low tephra content, the eruption plume reached a relatively high altitude (16 km), attributed to vaporisation of seawater in the shallow submarine environment (Maeno et al., 2022). Along with Hunga, these events demonstrate the potential for shallow subaqueous eruptions to produce water- or ice-rich, but tephra- and sulfur-poor upper tropospheric or stratospheric plumes.

Given the predominance of submarine volcanism on Earth, it is certain that many explosive submarine eruptions of similar or higher magnitude to the Hunga eruption must have occurred in prehistoric times. However, if low SO_2 output is a pervasive feature of these events, then they may be poorly preserved in ice core proxy records (Wu et al., 2025), unless they also involve a significant subaerial (magmatic) component. The Santorini-Kolumbo complex (Aegean Sea, Greece) is one example of a shallow, submarine volcanic system that has been investigated in some detail. Deposits of the Late Bronze-Age (~1610 BCE) Minoan, caldera-forming eruption of Santorini (VEI 7) include Surtseyan ashfall, indicating phreatomagmatic activity when seawater gained access to the vent (Bond and Sparks, 1976). The 1650 CE submarine eruption of Kolumbo (7 km north-east of Santorini) was a VEI 5 event that generated a destructive tsunami (Cantner et al., 2014; Ulvrova et al., 2016). More recent investigations at Santorini have found evidence for a VEI 5 explosive submarine eruption in 726 CE (Preine et al., 2024), indicating that such events may be more common than previously recognised.

1.3.1 Comparison with the 1883 Krakatau eruption

Several studies have proposed the August 1883 eruption of Krakatau as a close analog of the 15 January 2022 Hunga eruption. This is based primarily on the striking similarity between the atmospheric Lamb waves and audible sounds generated by the paroxysmal Hunga explosion (~04:15 UTC on 15 January 2022) and the climactic caldera-forming event at Krakatau on 27 August 1883 (Wright et al., 2022; Matoza et al., 2022; Vergoz et al., 2022), supporting a similar eruptive process. During their climactic phases, the Hunga and Krakatau eruptions both produced at least 4 or 5 discrete, loud and energetic explosions (Self and Rampino, 1981; Self, 1992; Madden-Nadeau et al., 2021; Astafyeva et al., 2022; Purkis et al., 2023), intense lightning (Verbeek, 1885; Van Eaton et al.,

2023), maximum plume altitudes exceeding 40 km (Verbeek, 1884; Self, 1992; Proud et al., 2022), and globally observed tsunami waves (Lynett et al., 2022).

The final phase of the Krakatau eruption on 26–27 August involved at least four powerful explosions, and ejected a total of 18–21 km^3 (9–10 km^3 DRE; VEI 6) of rhyodacite ejecta (Verbeek, 1884; Self and Rampino, 1981), roughly twice the volume of the 2022 Hunga (and 1991 Pinatubo) eruption deposits and more silicic in composition than 2022 Hunga andesite. Most of the Krakatau deposits were emplaced as PDCs that entered the ocean (Verbeek, 1884), causing destructive tsunamis responsible for most of the ~36,000 fatalities around the Sunda Straits, and hot ash-cloud surges that decoupled from the PDCs and moved 40 km across the ocean surface to Sumatra (Self and Rampino, 1981; Sigurdsson et al., 1991; Self, 1992; Carey et al., 1996). Similar voluminous PDCs entering the ocean may have caused the tsunamis observed during the Hunga eruption (Seabrook et al., 2023; Clare et al., 2023; Purkis et al., 2023).

At Krakatau and Hunga, it has been proposed that the likely origin of the PDCs was collapse of the eruption column during phases of high mass flux, most likely coincident with caldera collapse (Figure 1-6; Self, 1992; Clare et al., 2023). The relatively coarse-grained nature of the Krakatau PDC deposits (ignimbrites) and paleomagnetic evidence for high emplacement temperature argue against significant magma-seawater interaction during the climactic phase of the 1883 eruption, indicating that the eruption was not phreatoplinian (Self and Rampino, 1981; Mandeville et al., 1994; Mandeville et al., 1996b). Rather, it is thought that the Krakatau PDCs were generated by a subaerial vent (via column collapse) and then entered the ocean (Sigurdsson et al., 1991), in contrast to the Hunga PDCs that were formed via collapse of an eruption column issuing from a submarine vent (Seabrook et al., 2023; Clare et al., 2023).

At Krakatau, maximum eruption column heights (estimated to be ~40–50 km) occurred during the ignimbrite phase in the morning of 27 August, and were probably supplied by co-ignimbrite plumes rising above PDCs and ash-cloud surges as they swept across (and into) the ocean (Self and Rampino, 1981; Self, 1992). These co-ignimbrite plumes would have been humidified through entrainment of moist tropospheric air and (presumably) some evaporated seawater (Carey et al., 1996; Dartevelle et al., 2002). Textural evidence suggests that the Krakatau PDCs did not significantly mix with seawater (Sigurdsson et al., 1991), so the role of seawater evaporation is debatable, although some steam was likely produced at the seawater-flow interface (Carey et al., 1996). Had the PDCs mixed with seawater, Mandeville et al. (1996b) estimated that this could have yielded ~4200 Tg of steam (and ~7.6 Tg SO_2 from seawater sulfate).

At Hunga, in contrast, evaporated seawater rising above submarine PDCs or phreatomagmatic jets has been postulated as the main source of heat that drove the plume to an altitude of 58 km, requiring ~2900 Tg of steam (Mastin et al., 2024). Hence, during both the 2022 Hunga and 1883 Krakatau eruptions, PDCs likely played a role in the generation of stratospheric plumes, but the submarine vent at Hunga would have favored a phreatoplinian eruption style without significant subaerial co-ignimbrite plumes as invoked at Krakatau. Stratospheric injection via large co-ignimbrite plumes is a hallmark of the highest magnitude subaerial explosive eruptions (VEI 6+), with direct injection via Plinian eruption columns dominant in smaller eruptions (Rampino and Self, 1982; Dartevelle et al., 2002). At Hunga, one could envisage a process whereby submarine eruption of hot magma mixing with seawater generated large quantities of steam, but rapid burial by freshly erupted material delayed the explosive expansion until sufficient overpressure was achieved, producing repetitive strong explosions via a process originally proposed by Walker (1979) for explosions generated by ocean-entering PDCs.

The 1883 Krakatau eruption destroyed most of the pre-existing island (including the Danan and Perbuwatan cones that were the main eruption vents) and formed a ~250 m deep submarine caldera (Deplus et al., 1995); shallower than the ~850 m deep 2022 Hunga caldera formed by ~700 m of subsidence (Figure 1.6). However, taking into account the pre-eruption elevation of the Krakatau edifice (~1500 ft or 500 m asl at Danan; Symons et al., 1888), the vertical change in height due to caldera collapse at Hunga and Krakatau was similar. As noted above, it remains unclear whether the void excavated by the Hunga eruption was formed entirely by caldera collapse or phreatomagmatic explosive activity or a combination of processes. Nevertheless, the similarity between the geophysical signals produced by the paroxysmal Hunga and Krakatau explosions, coupled with the suite of observations available for Hunga, may improve our understanding of the Krakatau eruption.

The atmospheric and climate impacts of the 1883 Krakatau eruption were notably different from the

2022 Hunga eruption, apparently due to a major difference in stratospheric SO_2 loading. The Krakatau eruption famously produced vivid sunsets and other atmospheric optical effects that were observed at various locations around the world up to a year after the eruption (Symons et al., 1888), whereas the Hunga eruption was unremarkable in this regard (Carn et al., 2022). This can be attributed to the much higher stratospheric sulfur loading by the 1883 Krakatau eruption, which produced clear bipolar sulfate anomalies in Greenland and Antarctic ice cores. Based on the Greenland Ice Sheet Project 2 (GISP2) ice core sulfate anomaly, Zielinski (1995) estimated a maximum stratospheric sulfate aerosol loading of 46 Tg for Krakatau, equivalent to ~30 Tg SO_2. Although such estimates are subject to significant uncertainty, this suggests a stratospheric sulfur loading of a similar order of magnitude to the 1991 Pinatubo eruption. Using petrological data, Mandeville et al. (1996b) estimated a significantly lower eruptive SO_2 yield of ~6 Tg; they suggested that ~8 Tg SO_2 potentially derived from evaporated seawater and degassing of unerupted magma would resolve some of the discrepancy. However, if the potential contribution of a sulfur-rich pre-eruptive gas phase in the Krakatau magma is considered, SO_2 yields of up to 160 Tg are possible (Scaillet et al., 2003).

Global mean stratospheric aerosol optical depth (SAOD) values reconstructed from sulfate anomalies in ice cores reach a maximum of about 0.12 after the Krakatau eruption (Toohey and Sigl, 2017), similar to the post-Pinatubo SAOD. In contrast, the relatively low SO_2 emissions from the 2022 Hunga eruption suggest that the frequency of high-magnitude explosive submarine (i.e., phreatoplinian) eruptions may be poorly represented in the ice core record (Wu et al., 2025). As noted earlier (Section 1.1.3), the 1040–1180 CE Hunga caldera-forming event has been tentatively linked to a 1108 CE sulfate anomaly in ice cores and significant (>1°C) global cooling (Cronin et al., 2017; Sigl et al., 2015); if this match is confirmed, it would suggest that the previous caldera- forming event at Hunga may have been more subaerial in character than the 2022 eruption, i.e., more similar to the 1883 Krakatau eruption.

The 2022 Hunga eruption emitted ~0.5–1 Tg of SO_2 (Carn et al., 2022; Sellitto et al., 2022; Sellitto et al., 2024), which yielded 1.6 ± 0.5 Tg of stratospheric sulfate aerosol (Sellitto et al., 2024). Whilst the timing and magnitude of SO_2 emissions from Hunga is well-constrained by satellite observations, the ice core record can only provide a reasonable estimate of the total SO_2 loading for the 1883 Krakatau eruption, and cannot resolve SO_2 emissions by individual events in the ~4 month-long eruption sequence (May–August 1883), including the multiple major explosions during the 22–24 hour climactic phase on 26–27 August (Self and Rampino, 1981; Self, 1992; Madden-Nadeau et al., 2021). Hence, the specific SO_2 loading associated with the paroxysmal Krakatau explosion at ~10:00 am (local time) on 27 August 1883 (the Hunga analog) is unknown. Self (1992) notes that atmospheric optical effects indicative of stratospheric aerosols (solar haloes and blue moons) were reported as early as July 1883 from almost 3000 km away, and were most likely sourced from Krakatau. Further optical effects were observed in South Africa in mid-August 1883, prior to the climactic phase of the eruption (Self, 1992). This suggests that significant stratospheric SO_2 injection had likely already occurred prior to 26–27 August 1883.

The main, lasting impact of the 2022 Hunga eruption was hydration of the tropical stratosphere due to the direct injection of ~150 Tg of WV (Millán et al., 2022). This is likely only a small fraction of the total amount of WV initially present in the volcanic plume (estimated to be ~2900 Tg during the first hour; Mastin et al., 2024; Wu et al., 2025), most of which was lost by freezing and ice fallout during plume ascent. Based on petrological data, total magmatic water emissions during the 1883 Krakatau eruption have been estimated at ~920 Tg (Mandeville et al., 1996a), compared to ~320 Tg magmatic water degassed from Hunga (Wu et al., 2025).

In their modelling study of the potential climate impact of stratospheric WV injection, Joshi and Jones (2009) assumed a WV injection of 500 Tg by the 1883 Krakatau eruption with a constant mixing ratio between 0 and 40 km altitude (i.e., not all the injected WV was stratospheric); the injected mass was based solely on estimates of water emissions by the 1991 Pinatubo eruption (minimum ~500 Tg magmatic water; Gerlach et al., 1996). Hence, the total stratospheric WV injection by the 1883 Krakatau eruption remains poorly constrained, but given the higher magmatic water emissions than Hunga, plus potential contributions from WV entrained into co-ignimbrite plumes (estimated to be ~2500 Tg for Pinatubo; Dartevelle et al., 2002) and seawater evaporated by PDCs (potentially up to 4200 Tg; Mandeville et al., 1996a), a stratospheric WV injection similar to or larger than Hunga seems plausible.

Further evidence for similarities in the evolution of the Hunga and Krakatau stratospheric aerosols stems from widespread purple twilight observations in the tropics after the 1883 Krakatau eruption, indicating that the aerosol descended from 32 km to 24 km in the first weeks post-eruption (Symons et al., 1888; Pernter, 1889; Wexler, 1951). The Hunga plume descent rate was remarkably similar (Sellitto et al., 2022; Legras et al., 2022), consistent with strong radiative cooling induced by stratospheric WV. Estimates of stratospheric WV injection are important in the context of discrepancies between the observed and modelled cooling following the 1883 Krakatau eruption (Knutson et al., 2006), whereby warming due to injected WV would partially offset surface cooling due to sulfate aerosols (Joshi and Jones, 2009). A similar interaction between the effects of WV and sulfate aerosols has been proposed for the 2022 Hunga eruption (Chapter 7; e.g., Sellitto et al., 2022; Schoeberl et al., 2024).

1.3.2 Summary of recent eruptions and large wildfires with radiative impacts

In the decade prior to the 2022 Hunga eruption, multiple stratospheric events—including extreme wildfires and explosive volcanic eruptions—significantly influenced the stratospheric aerosol layer and SAOD. Figure 1.8 and Table 1.3 show that between 2012 and 2022, the stratosphere was frequently impacted by either volcanic eruptions or strong wildfire events, primarily injected into the Upper Troposphere and Lower Stratosphere (UTLS) via pyro-cumulonimbus clouds (pyro-Cbs) forming above intense wildfires (Fromm et al., 2010).

Large wildfire events inject aerosols with a different composition compared to volcanic eruptions. These fire-derived aerosols typically enter the UTLS through intense pyro-convection (Fromm et al., 2010). Whereas volcanic aerosols vary in sulfur and ash content (Muser et al., 2020) and can be influenced by water content (as for the Hunga eruption), wildfire plumes are dominated by carbonaceous particles, such as black carbon. Radiative heating of these particles can lead to further lofting, enhancing their atmospheric lifetime and climatic influence (Yu et al., 2019; Ohneiser et al., 2023).

The main events in 2012–2022 with significant stratospheric impact are summarised below.

Kelut 2014 (Java, Indonesia): In February 2014, the tropical Kelut volcano (8°S, 112°E) erupted, injecting ~0.2 Tg SO_2 to altitudes above 20 km and generating an estimated global, stratospheric radiative forcing of -0.2 W/m^2. Part of the aerosol plume was entrained in the tropical pipe, impacting the stratosphere for several years (Friberg et al., 2018). Volcanic ash played a significant role for approximately three months after the injection (Vernier et al., 2016), impacting the stratospheric SO_2 lifetime and aerosol optical properties (Zhu et al., 2020).

Calbuco 2015 (Chile): Calbuco (41°S, 73°W) erupted in April 2015, emitting approximately 0.4 Tg of SO_2. sulfate aerosols were transported southwards, enhancing polar ozone depletion (Stone et al., 2017; Zhu et al., 2018). Reactive field campaigns, including airborne aerosol observations on small balloons, took place on Réunion Island within a month of the Calbuco eruption (Bègue et al., 2017), similar to the subsequent response activated after the 2022 Hunga eruption. Réunion was more favorably located for the Hunga eruption response, being directly downwind of the volcano at a similar latitude (~20°S).

British Columbia Fires 2017 (Canada): Intense wildfires in British Columbia, Canada, injected significant amounts of smoke into the lower stratosphere through pyro-convection in August 2017 (Khaykin et al., 2018). The plume circled the Earth in the northern hemisphere, with record-breaking aerosol perturbations 2–5 km above the tropopause observed over Europe in August 2017 (Ansmann et al., 2018). The aerosol plume was lofted by radiative heating to an altitude of 23 km (Yu et al., 2019). Das et al. (2021) estimated a clear-sky, global top-of-the-atmosphere (TOA) radiative forcing of -0.03 W/m² due to the stratospheric smoke aerosols.

Ambae 2018 (Vanuatu): Two eruptions at Ambae volcano (15°S, 168°E) in April and July 2018 injected ~0.4 Tg SO_2 into the lower stratosphere with injection altitudes of up to 18 km, impacting both hemispheres with elevated aerosol concentrations (Kloss et al., 2020). The respective tropical (20°N to 20°S) radiative forcing is estimated at approximately -0.13 W/m² (Malinina et al., 2021). Although the SO_2 injected was only slightly lower than that of the Hunga eruption (~0.6–1 Tg; Carn et al., 2022; Sellitto et al., 2024), Figure 1.8 shows that the Ambae eruptions had the least impact on SAOD over the past decade. Two factors likely explain this: (1) the significantly lower injection altitude at Ambae, which allowed aerosols to settle into the troposphere more quickly, and (2) the co-injection of water during the Hunga eruption, which contributed to rapid formation of sulfate aero-

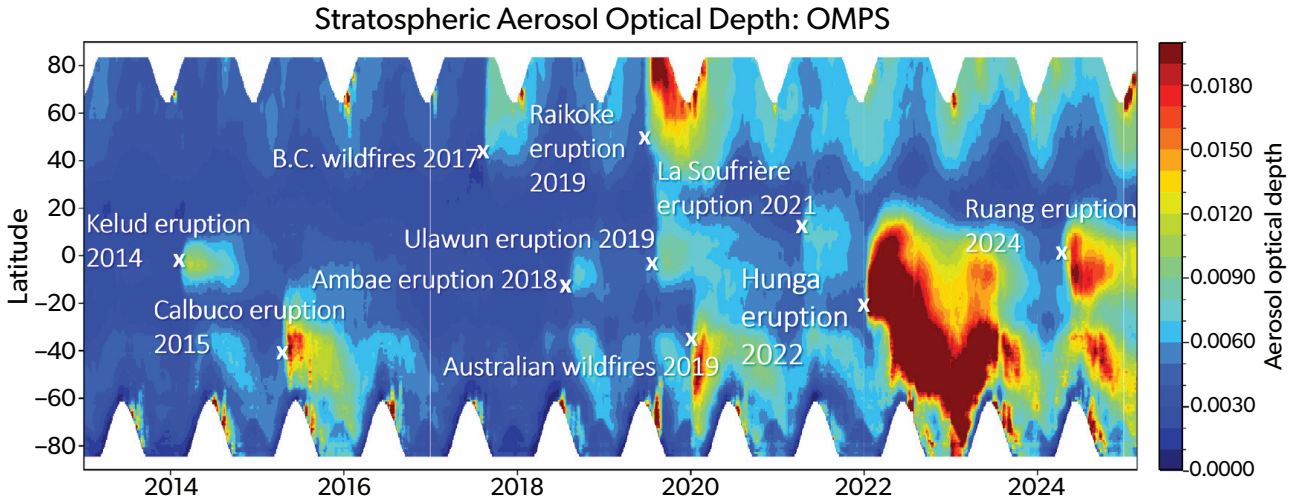

Figure 1.8: *Stratospheric Aerosol Optical Depth (SAOD) at 675 nm from Suomi National Polar-orbiting Partnership/Ozone Mapping and Profiler Suite (SNPP/OMPS) Limb-profiler (LP) version 2.0 (Taha et al., 2021) aerosol extinction observations (2012–2025). Periods of major stratospheric aerosol events, including extreme wildfires and volcanic eruptions, are indicated.*

Table 1.3: *Significant stratospheric aerosol optical depth (SAOD) perturbations in the decade preceding the 2022 Hunga eruption.*

Eruption/Wildfire	Date	Latitude	SO_2 loading (Tg)	Peak SAOD[1]
Kelut (Indonesia)	Feb 2014	8°S	0.2	0.007
Calbuco (Chile)	Apr 2015	41°S	0.4	0.01
BC Fires (Canada)	Aug 2017	42°N	–	0.006
Ambae/Aoba (Vanuatu)	Apr–Jul 2018	15°S	0.4	0.009
Raikoke (Russia)	Jun 2019	48°N	1.4	0.015
Ulawun (Papua New Guinea)	Jun–Aug 2019	5°S	0.4	0.015*
Australian Fires	Dec 2019	27–38°S	–	0.016*
Taal (Philippines)	Jan 2020	14°N	0.2	0.016*
La Soufrière (St. Vincent)	Apr 2021	13°N	0.6	0.01

[1]Monthly mean SAOD in the 60°S–60°N latitude band from the GloSSAC database (Kovilakam et al., 2020).

* The Ulawun, Australian Fire, and Taal SAOD signals merge with the earlier Raikoke anomaly.

sols (Zhu et al., 2022; Sellitto et al., 2024; Asher et al., 2023).

Raikoke (Kuril Islands, Russia) and Ulawun (Papua New Guinea) 2019: The Raikoke (48°N, 153°E) and Ulawun (5°S, 151°E) volcanoes produced near-coincident eruptions in the northern hemisphere summer of 2019. The Raikoke eruption injected around 1.5 Tg of SO_2 and 0.7 Tg of fine ash, leading to a global monthly mean radiative forcing of -0.17 W/m² (Prata et al., 2022; Vernier et al., 2024). During two Ulawun eruptions (June and August 2019), a total of ~0.4 Tg SO_2 was injected (Carn, 2024), resulting in an all-sky global radiative forcing estimate of -0.05 W/m² (Kloss et al., 2021). While the Raikoke plume was primarily distributed in the northern hemisphere, the tropical Ulawun eruptions affected the tropical stratosphere and southern mid-latitudes. A large phreatomagmatic eruption of Taal volcano (Philippines) in January 2020 (Van Eaton et al., 2022; Perttu et al., 2023) injected an additional ~0.2 Tg SO_2 into the stratosphere, overprinting the SAOD signals from the 2019 Raikoke and Ulawun eruptions and the 2019–2020 Australian Fires.

Australian Fires 2019/2020, the Black Summer': During the wildfire season in Australia, a series of pyro-Cb events injected gases and aerosols into the UTLS around New Year 2019/2020. The resulting aerosol plume caused abrupt lower stratospheric warming, not observed since Pinatubo, and led to extended recovery of the Antarctic ozone layer (Yu et al., 2021; Damany-Pearce et al., 2022; Solomon et al., 2022; Ohneiser et al., 2022). Peak TOA radiative forcing values are estimated at ~-0.3 W/m² based on satellite observations and microphysical properties (Sellitto

et al., 2022). During the Australian fires, self-induced smoke vortices' were observed, which carried ozone holes and persisted for several months (Khaykin et al., 2020; Kablick et al., 2020). Similar features may also result from volcanic eruptions with ash injections, as seen after the Raikoke eruption (Lestrelin et al., 2021; Khaykin et al., 2022). Both the 2017 British Columbia fires and the 2019–2020 Australian fires are among the strongest recorded wildfires with global stratospheric impact, comparable to moderate volcanic eruptions.

La Soufrière 2021 (St. Vincent and the Grenadines): The eruption at La Soufrière (13.3°N, 61.2°W) occurred ~9 months before the 2022 Hunga eruption, providing context for the pre-Hunga stratospheric state. The 2021 La Soufrière eruption injected an estimated 0.6 Tg SO_2 (Taylor et al., 2023), reaching altitudes between 18 and 20 km (Horváth et al., 2022). The aerosol plume contributed to an increase in smaller particles (<400 nm). The global 1-year average radiative forcing was calculated at -0.08 W/m² for clear-sky conditions and -0.04 W/m² for all-sky conditions, affecting both the tropics and northern mid-latitudes (Li et al., 2023). As shown in Figure 1.8 using OMPS-LP measurements, SAOD enhancements following the La Soufrière eruption had not entirely returned to background levels at the time of the Hunga eruption in January 2022. Compared to the background SAOD in the tropics in 2017/2018 (~0.003), the stratospheric aerosol layer remained elevated at ~0.005, roughly double the baseline value.

1.4 Summary and conclusions

As the first high-magnitude, explosive submarine eruption in the modern instrumental or satellite eras, the 15 January 2022 Hunga eruption has provided a wealth of new observations of such events that will inform responses to, and modelling of, future analogous eruptions. The Hunga eruption may yet be categorised as a phreatoplinian eruption, although we note that past eruptions in this category have been classified based solely on the eruption deposits (e.g., high proportions of fine ash particles). The Hunga eruption, where subaerial tephra deposits were limited, provides a new set of geophysical observations that may be used to further refine the criteria for a phreatoplinian event, and classify future phreatomagmatic eruptions in this category.

On the basis of observations made during the 2022 Hunga eruption, we can draw the following preliminary conclusions:

- Future phreatoplinian eruptions may not produce climatically significant SO_2 loading detectable by satellites (>5 Tg), yet may still have significant impacts on atmospheric chemistry, circulation, and climate. Volcanic eruption response plans used by NASA and others may need to be updated to account for such events, e.g., by using umbrella cloud growth rates or mass eruption rates (which are easily determined using geostationary satellite data) as additional criteria for eruption response.
- Based on observations of Hunga and other recent phreatomagmatic eruptions, phreatoplinian eruption clouds are likely to be ash-poor, although the presence of very fine ash particles produced by phreatomagmatic fragmentation remains possible. In water-rich eruptions, ash particles are rapidly stripped from the plume by hydrometeors.
- Phreatoplinian eruptions may inject water vapor, SO_2, volcanic ash, and other constituents (e.g., HCl, sea salt) into the stratosphere, potentially to very high altitudes (>50 km). The injection heights and vertical profiles of these constituents may differ temporally and spatially due to complex eruption processes (e.g., if water vapor is derived from seawater evaporation above submarine PDCs, which releases little SO_2).
- Regardless of their initial vertical profiles, constituent profiles are expected to rapidly evolve in a water-rich, phreatoplinian eruption (more rapidly than a magmatic eruption) as water freezes and/or condenses (which is dependent on plume altitude, determining temperature and water saturation). Liquid water and ice would rapidly remove volcanic ash, leaving some water vapor and SO_2. The remaining SO_2 would begin rapidly converting to sulfate aerosol in water-rich layers.
- The injection of sea salt derived from evaporated seawater may lead to enhanced concentrations of halogens (Cl, Br), with consequences for atmospheric chemistry.

References

Abbott, D. and J. L. Rubenstone (2024). 'The abundance of submarine volcanism in arcs'. *Volcanica*, 7, pp. 447–459. DOI: 10.30909/vol.07.02.447459.

Ansmann, A., H. Baars, A. Chudnovsky, I. Mattis, I. Veselovskii, M. Haarig, P. Seifert, R. Engelmann and U. Wandinger (2018). 'Extreme levels of Canadian wildfire smoke in the stratosphere over central Europe on 21–22 August 2017'. *Atmos. Chem. Phys.*, 18, pp. 11831–11845. DOI: 10.5194/acp-18-11831-2018.

Asher, E., M. Todt, K. Rosenlof, T. Thornberry, R.-S. Gao, G. Taha, P. Walter, S. Alvarez, J. Flynn, S. M. Davis et al. (2023). 'Unexpectedly rapid aerosol formation in the Hunga Tonga plume'. *Proc. Natl. Acad. Sci.*, 120, e2219547120. DOI: 10.1073/pnas.2219547120.

Astafyeva, E., B. Maletckii, T. D. Mikesell, E. Munaibari, M. Ravanelli, P. Coisson, F. Manta and L. Rolland (2022). 'The 15 January 2022 Hunga Tonga Eruption History as Inferred From Ionospheric Observations'. *Geophys. Res. Lett.*, 49, e2022GL098827. DOI: 10.1029/2022GL098827.

Babu, S. R. and N.-H. Lin (2023). 'Extreme Heights of 15 January 2022 Tonga Volcanic Plume and Its Initial Evolution Inferred from COSMIC-2 RO Measurements'. *Atmosphere*, 14, 121. DOI: 10.3390/atmos14010121.

Baron, A., P. Chazette, S. Khaykin, G. Payen, N. Marquestaut, N. Bègue and V. Duflot (2023). 'Early Evolution of the Stratospheric Aerosol Plume Following the 2022 Hunga Tonga-Hunga Ha'apai Eruption: Lidar Observations From Reunion (21°S, 55°E)'. *Geophys. Res. Lett.*, 50, e2022GL101751. DOI: 10.1029/2022gl101751.

Bègue, N., D. Vignelles, G. Berthet, T. Portafaix, G. Payen, F. Jégou, H. Benchérif, J. Jumelet, J.-P. Vernier, T. Lurton et al. (2017). 'Long-range transport of stratospheric aerosols in the Southern Hemisphere following the 2015 Calbuco eruption'. *Atmos. Chem. Phys.*, 17, pp. 15019–15036. DOI: 10.5194/acp-17-15019-2017.

Beinart, R. A., S. M. Arellano, M. Chaknova, J. Meagher, A. J. Davies, J. Lopresti, E. J. Cowell, M. Betters, T. M. Ladd, C. Q. Plowman et al. (2024). 'Deep seafloor hydrothermal vent communities buried by volcanic ash from the 2022 Hunga eruption'. *Commun. Earth Environ.*, 5, 254. DOI: 10.1038/s43247-024-01411-w.

Bohnenstiehl, D. R., R. P. Dziak, H. Matsumoto and T.-K. Lau (2013). 'Underwater acoustic records from the March 2009 eruption of Hunga Ha'apai–Hunga Tonga volcano in the Kingdom of Tonga'. *J. Volcanol. Geotherm. Res.*, 249, pp. 12–24. DOI: 10.1016/j.jvolgeores.2012.08.014.

Bond, A. and R. S. J. Sparks (1976). 'The Minoan eruption of Santorini, Greece'. *J. Geol. Soc.*, 132, pp. 1–16. DOI: 10.1144/gsjgs.132.1.0001.

Borrero, J. C., S. J. Cronin, F. H. Latu'ila, P. Tukuafu, N. Heni, A. M. Tupou, T. Kula, O. Fa'anunu, C. Bosserelle, E. Lane et al. (2023). 'Tsunami Runup and Inundation in Tonga from the January 2022 Eruption of Hunga Volcano'. *Pure Appl. Geophys.*, 180, pp. 1–22. DOI: 10.1007/s00024-022-03215-5.

Brandl, P. A., F. Schmid, N. Augustin, I. Grevemeyer, R. J. Arculus, C. W. Devey, S. Petersen, M. Stewart, H. Kopp and M. D. Hannington (2020). 'The 6–8 Aug 2019 eruption of 'Volcano F' in the Tofua Arc, Tonga'. *J. Volcanol. Geotherm. Res.*, 390, 106695. DOI: 10.1016/j.jvolgeores.2019.106695.

Brenna, M., S. J. Cronin, I. E. M. Smith, A. Pontesilli, M. Tost, S. Barker, S. Tonga'onevai, T. Kula and R. Vaiomounga (2022). 'Post-caldera volcanism reveals shallow priming of an intra-ocean arc andesitic caldera: Hunga volcano, Tonga, SW Pacific'. *Lithos*, 412-413, 106614. DOI: 10.1016/j.lithos.2022.106614.

Bryan, S. E., A. Cook, J. P. Evans, P. W. Colls, M. G. Wells, M. G. Lawrence, J. S. Jell, A. Greig and R. Leslie (2004). 'Pumice rafting and faunal dispersion during 2001–2002 in the Southwest Pacific: record of a dacitic submarine explosive eruption from Tonga'. *Earth Planet. Sci. Lett.*, 227, pp. 135–154. DOI: 10.1016/j.epsl.2004.08.009.

Cahalan, R. and J. Dufek (2021). 'Explosive submarine eruptions: The role of condensable gas jets in underwater eruptions'. *J. Geophys. Res.*, 126, e2020JB020969. DOI: 10.1029/2020JB020969.

Cantner, K., S. Carey and P. Nomikou (2014). 'Integrated volcanologic and petrologic analysis of the 1650 AD eruption of Kolumbo submarine volcano, Greece'. *J. Volcanol. Geotherm. Res.*, 269, pp. 28–43. DOI: 10.1016/j.jvolgeores.2013.10.004.

Carey, R., S. A. Soule, M. Manga, J. D. L. White, J. McPhie, R. Wysoczanski, M. Jutzeler, K. Tani, D. Yoerger, D. Fornari et al. (2018). 'The largest deep-ocean silicic volcanic eruption of the past century'. *Sci. Adv.*, 4, e1701121. DOI: 10.1126/sciadv.1701121.

Carey, S. and H. Sigurdsson (1986). 'The 1982 eruptions of El Chichon volcano, Mexico (2): Observations and numerical modelling of tephra-fall distri-

bution'. *Bull. Volcanol.*, 48, pp. 127–141. DOI: 10.1007/BF01046547.

Carey, S., H. Sigurdsson, C. Mandeville and S. Bronto (1996). 'Pyroclastic flows and surges over water: an example from the 1883 Krakatau eruption'. *Bull. Volcanol.*, 57, pp. 493–511. DOI: 10.1007/BF00304435.

Carn, S. A., N. A. Krotkov, B. L. Fisher and C. Li (2022). 'Out of the blue: volcanic SO_2 emissions during the 2021-2022 Hunga Tonga-Hunga Ha'apai eruptions'. *Front. Earth Sci.*, 13. DOI: 10.3389/feart.2022.976962.

Carn, S. (2024). *Multi-Satellite Volcanic Sulfur Dioxide L4 Long-Term Global Database V4*. Goddard Earth Science Data and Information Services Center (GES DISC), Greenbelt, MD, USA. Last access: 20 March 2025. DOI: 10.5067/MEASURES/SO2/DATA405.

Carn, S. A., P. A. Newman, V. Aquila, H. Gonnermann and J. Dufek (2021). 'Anticipating climate impacts of major volcanic eruptions'. *Eos*, 102. DOI: 10.1029/2021EO162730.

Carr, J. L., Á. Horváth, D. L. Wu and M. D. Friberg (2022). 'Stereo Plume Height and Motion Retrievals for the Record-Setting Hunga Tonga-Hunga Ha'apai Eruption of 15 January 2022'. *Geophys. Res. Lett.*, 49, e2022GL098131. DOI: 10.1029/2022gl098131.

Carvajal, M., I. Sepúlveda, A. Gubler and R. Garreaud (2022). 'Worldwide signature of the 2022 Tonga volcanic tsunami'. *Geophys. Res. Lett.*, 49, e2022GL098153. DOI: 10.1029/2022gl098153.

Cas, R. A. F. and J. M. Simmons (2018). 'Why deep-water eruptions are so different from subaerial eruptions'. *Front. Earth Sci.*, 6, 198. DOI: 10.3389/feart.2018.00198.

Chaknova, M., T. Giachetti, J. Paredes-Mariño, A. Soule, A. R. Van Eaton, R. Beinart, M. Crundwell, S. J. Cronin, M. Jutzeler, K. E. Fauria et al. (2025). 'How did westward volcaniclastic deposits accumulate in the deep sea following the January 2022 eruption of Hunga volcano?' *Geochem. Geophys. Geosyst.*, 26, e2024GC011629. DOI: 10.1029/2024GC011629.

Clare, M. A., I. A. Yeo, S. Watson, R. Wysoczanski, S. Seabrook, K. Mackay, J. E. Hunt, E. Lane, P. J. Talling, E. Pope et al. (2023). 'Fast and destructive density currents created by ocean-entering volcanic eruptions'. *Science*, 381, pp. 1085–1092. DOI: 10.1126/science.adi3038.

Colombier, M., B. Scheu, F. B. Wadsworth, S. Cronin, J. Vasseur, K. J. Dobson, K.-U. Hess, M. Tost, T. I. Yilmaz, C. Cimarelli et al. (2018). 'Vesiculation and quenching during Surtseyan eruptions at Hunga Tonga-Hunga Ha'apai Volcano, Tonga'. *J. Geophys Res.*, 123, pp. 3762–3779. DOI: 10.1029/2017JB015357.

Colombier, M., I. A. Ukstins, S. Tegtmeier, B. Scheu, S. J. Cronin, S. Thivet, J. Paredes-Mariño, C. Cimarelli, K.-U. Hess, T. Kula et al. (2023). 'Atmosphere injection of sea salts during large explosive submarine volcanic eruptions'. *Sci. Rep.*, 13, 14435. DOI: 10.1038/s41598-023-41639-8.

Cronin, J. F. (1971). 'Recent volcanism and the stratosphere'. *Science*, 172, pp. 847–849. DOI: 10.1126/science.172.3985.847.

Cronin, S., M. Brenna, I. Smith, S. Barker, M. Tost, M. Ford, S. Tonga'onevai, T. Kula and R. Vaiomounga (2017). 'New volcanic island unveils explosive past'. *Eos*, 98. DOI: 10.1029/2017EO076589.

Damany-Pearce, L., B. Johnson, A. Wells, M. Osborne, J. Allan, C. Belcher, A. Jones and J. Haywood (2022). 'Australian wildfires cause the largest stratospheric warming since Pinatubo and extend the lifetime of the Antarctic ozone hole'. *Sci. Rep.*, 12, 12665. DOI: 10.1038/s41598-022-15794-3.

Dartevelle, S., G. G. J. Ernst, J. Stix and A. Bernard (2002). 'Origin of the Mount Pinatubo climactic eruption cloud: Implications for volcanic hazards and atmospheric impacts'. *Geology*, 30, pp. 663–666. DOI: 10.1130/0091-7613(2002)030<0663:ootmpc>2.0.co;2.

Das, S., P. R. Colarco, L. D. Oman, G. Taha and O. Torres (2021). 'The long-term transport and radiative impacts of the 2017 British Columbia pyrocumulonimbus smoke aerosols in the stratosphere'. *Atmos. Chem. Phys.*, 21, pp. 12069–12090. DOI: 10.5194/acp-21-12069-2021.

Delgado, F., J. Kubanek, K. Anderson, P. Lundgren and M. Pritchard (2019). 'Physicochemical models of effusive rhyolitic eruptions constrained with InSAR and DEM data: A case study of the 2011-2012 Cordón Caulle eruption'. *Earth Planet. Sci. Lett.*, 524, 115736. DOI: 10.1016/j.epsl.2019.115736.

Deligne, N. I. and H. Sigurdsson (2015). 'Global Rates of Volcanism and Volcanic Episodes'. *Encyclopedia of Volcanoes, 2nd Ed.* Pp. 265–272. DOI: 10.1016/B978-0-12-385938-9.00014-6.

Delos Reyes, P. J., M. A. V. Bornas, D. Dominey-Howes, A. C. Pidlaoan, C. R. Magill and R. U. Solidum, Jr. (2018). 'A synthesis and review of historical eruptions at Taal Volcano, Southern Luzon, Philippines'.

Earth Sci. Rev., 177, pp. 565–588. DOI: 10.1016/j.Earscirev.2017.11.014.

Deplus, C., S. Bonvalot, D. Dahrin, M. Diament, H. Harjono and J. Dubois (1995). 'Inner structure of the Krakatau volcanic complex (Indonesia) from gravity and bathymetry data'. *J. Volcanol. Geotherm. Res.*, 64, pp. 23–52. DOI: 10.1016/0377-0273(94)00038-i.

Embley, R., Y. Tamura, S. Merle, T. Sato, O. Ishizuka, W. Chadwick, D. Wiens, P. Shore and R. Stern (2014). 'Eruption of South Sarigan seamount, Northern Mariana Islands: Insights into hazards from submarine volcanic eruptions'. *Oceanography*, 27, pp. 24–31. DOI: 10.5670/oceanog.2014.37.

Fauria, K. E., M. Jutzeler, T. Mittal, A. K. Gupta, L. J. Kelly, J. Rausch, R. Bennartz, B. Delbridge and L. Retailleau (2023). 'Simultaneous creation of a large vapor plume and pumice raft by a shallow submarine eruption'. *Earth Planet. Sci. Lett.*, 609, 118076. DOI: 10.1016/j.epsl.2023.118076.

Friberg, J., B. Martinsson, S. Andersson and O. Sandvik (2018). 'Volcanic impact on the climate – the stratospheric aerosol load in the period 2006–2015'. *Atmos. Chem. Phys.*, 18, pp. 11149–11169. DOI: 10.5194/acp-18-11149-2018.

Fromm, M., D. T. Lindsey, R. Servranckx, G. Yue, T. Trickl, R. Sica, P. Doucet and S. Godin-Beekmann (2010). 'The untold story of pyrocumulonimbus'. *Bull. Am. Meteorol. Soc.*, 91, pp. 1193–1209. DOI: 10.1175/2010bams3004.1.

Garvin, J. B., D. A. Slayback, V. Ferrini, J. Frawley, C. Giguere, G. R. Asrar and K. Andersen (2018). 'Monitoring and modeling the rapid evolution of Earth's newest volcanic island: Hunga Tonga Hunga Ha'apai (Tonga) using high spatial resolution satellite observations'. *Geophys. Res. Lett.*, 45, pp. 3445–3452. DOI: 10.1002/2017GL076621.

Gerlach, T. M., H. R. Westrich and R. B. Symonds (1996). 'Preeruption Vapor in Magma of the Climactic Mount Pinatubo Eruption: Source of the Giant Stratospheric Sulfur Dioxide Cloud'. *Fire and Mud: Eruptions and Lahars of Mount Pinatubo, Philippines.* Ed. by C. Newhall and R. Punongbayan. University of Washington Press, Seattle, USA.

Glaze, L. S., S. M. Baloga and L. Wilson (1997). 'Transport of atmospheric water vapor by volcanic eruption columns'. *J. Geophys. Res.*, 102, pp. 6099–6108. DOI: 10.1029/96JD03125.

Global Volcanism Program (2009). *Report on Hunga Tonga-Hunga Ha'apai (Tonga) (Venzke, E. A., and Wunderman, R., eds.)* Bulletin of the Global Volcanism Network, 34:2. Smithsonian Institution. DOI: 10.5479/si.GVP.BGVN200902-243040.

Global Volcanism Program (2022a). *Report on Hunga Tonga-Hunga Ha'apai (Tonga) (Bennis, K. L., and Venzke, E., eds.)* Bulletin of the Global Volcanism Network, 47:3. Smithsonian Institution. DOI: 10.5479/si.GVP.BGVN202203-243040.

Global Volcanism Program (2022b). *Report on Hunga Tonga-Hunga Ha'apai (Tonga) (Crafford, A. E., and Venzke, E., eds.)* Bulletin of the Global Volcanism Network, 47:2. Smithsonian Institution. DOI: 10.5479/si.GVP.BGVN202202-243040.

Global Volcanism Program (2024). *Volcanoes of the World (v. 5.2.8; 6 May 2025).* Distributed by Smithsonian Institution, compiled by Venzke, E. DOI: 10.5479/si.GVP.VOTW5-2024.5.2.

Green, D. N., L. G. Evers, D. Fee, R. S. Matoza, M. Snellen, P. Smets and D. Simons (2013). 'Hydroacoustic, infrasonic and seismic monitoring of the submarine eruptive activity and sub-aerial plume generation at South Sarigan, May 2010'. *J. Volcanol. Geotherm. Res.*, 257, pp. 31–43. DOI: 10.1016/j.jvolgeores.2013.03.006.

Gupta, A. K., R. Bennartz, K. E. Fauria and T. Mittal (2022). 'Eruption chronology of the December 2021 to January 2022 Hunga Tonga-Hunga Ha'apai eruption sequence'. *Commun. Earth Environ.*, 3, 314. DOI: 10.1038/s43247-022-00606-3.

Henley, R. W., C. E. J. de Ronde, R. J. Arculus, G. Hughes, T.-S. Pham, A. S. Casas, V. Titov and S. L. Walker (2024). 'The 15 January 2022 Hunga (Tonga) eruption: A gas-driven climactic explosion'. *J. Volcanol. Geotherm. Res.*, 451, 108077. DOI: 10.1016/j.jvolgeores.2024.108077.

Horváth, Á., J. L. Carr, D. L. Wu, J. Bruckert, G. A. Hoshyaripour and S. A. Buehler (2022). 'Measurement report: Plume heights of the April 2021 La Soufrière eruptions from GOES-17 side views and GOES-16–MODIS stereo views'. *Atmos. Chem. Phys.*, 22, pp. 12311–12330. DOI: 10.5194/acp-22-12311-2022.

Houghton, B., J. White and A. Van Eaton (2015). 'Phreatomagmatic and Related Eruption Styles'. *Encyclopedia of Volcanoes, 2nd Ed.* Pp. 537–552. DOI: 10.1016/B978-0-12-385938-9.00030-4.

International Seismological Centre (2022). *On-line Bulletin.* DOI: 10.31905/D808B830.

Joshi, M. M. and G. S. Jones (2009). 'The climatic effects of the direct injection of water vapour into the stratosphere by large volcanic eruptions'. *Atmos.*

Chem. Phys., 9, pp. 6109–6118. DOI: 10.5194/acp-9-6109-2009.

Jutzeler, M., R. Marsh, R. J. Carey, J. D. L. White, P. J. Talling and L. Karlstrom (2014). 'On the fate of pumice rafts formed during the 2012 Havre submarine eruption'. *Nat. Commun.*, 5, 3660. DOI: 10.1038/ncomms4660.

Kablick, G. P. I., D. R. Allen, M. D. Fromm and G. E. Nedoluha (2020). 'Australian pyroCb smoke generates synoptic-scale stratospheric anticyclones'. *Geophys. Res. Lett.*, 47, e2020GL088101. DOI: 10.1029/2020GL088101.

Kelly, L. J., K. E. Fauria, M. Manga, S. J. Cronin, F. H. Latu'ila, J. Paredes-Mariño, T. Mittal and R. Bennartz (2024). 'Airfall volume of the 15 January 2022 eruption of Hunga volcano estimated from ocean color changes'. *Bull. Volcanol.*, 86, 59. DOI: 10.1007/s00445-024-01744-6.

Khaykin, S. M., S. Godin-Beekmann, A. Hauchecorne, J. Pelon, F. Ravetta and P. Keckhut (2018). 'Stratospheric smoke with unprecedentedly high backscatter observed by lidars above southern France'. *Geophys. Res. Lett.*, 45, pp. 1639–1646. DOI: 10.1002/2017GL076763.

Khaykin, S., B. Legras, S. Bucci, P. Sellitto, L. Isaksen, F. Tencé, S. Bekki, A. Bourassa, L. Rieger, D. Zawada et al. (2020). 'The 2019/20 Australian wildfires generated a persistent smoke-charged vortex rising up to 35 km altitude'. *Commun. Earth Environ.*, 1, 22. DOI: 10.1038/s43247-020-00022-5.

Khaykin, S., A. Podglajen, F. Ploeger, J.-U. Grooß, F. Tence, S. Bekki, K. Khlopenkov, K. Bedka, L. Rieger, A. Baron et al. (2022). 'Global perturbation of stratospheric water and aerosol burden by Hunga eruption'. *Commun. Earth Environ.*, 3, 316. DOI: 10.1038/s43247-022-00652-x.

Kloss, C., G. Berthet, P. Sellitto, F. Ploeger, G. Taha, M. Tidiga, M. Eremenko, A. Bossolasco, F. Jégou, J.-B. Renard et al. (2021). 'Stratospheric aerosol layer perturbation caused by the 2019 Raikoke and Ulawun eruptions and their radiative forcing'. *Atmos. Chem. Phys.*, 21, pp. 535–560. DOI: 10.5194/acp-21-535-2021.

Kloss, C., P. Sellitto, B. Legras, J.-P. Vernier, F. Jégou, M. Venkat Ratnam, B. Suneel Kumar, B. Lakshmi Madhavan and G. Berthet (2020). 'Impact of the 2018 Ambae eruption on the global stratospheric aerosol layer and climate'. *J. Geophys. Res.*, 125, e2020JD032410. DOI: 10.1029/2020JD032410.

Kloss, C., P. Sellitto, J.-B. Renard, A. Baron, N. Bègue, B. Legras, G. Berthet, E. Briaud, E. Carboni, C. Duchamp et al. (2022). 'Aerosol characterization of the stratospheric plume from the volcanic eruption at Hunga Tonga 15 January 2022'. *Geophys. Res. Lett.*, 49, e2022GL099394. DOI: 10.1029/2022GL099394.

Knafelc, J., S. E. Bryan, M. W. M. Jones, D. Gust, G. Mallmann, H. E. Cathey, A. J. Berry, E. C. Ferré and D. L. Howard (2022). 'Havre 2012 pink pumice is evidence of a short-lived, deep-sea, magnetite nanolite-driven explosive eruption'. *Commun. Earth Environ.*, 3, 19. DOI: 10.1038/s43247-022-00355-3.

Knutson, T. R., T. L. Delworth, K. W. Dixon, I. M. Held, J. Lu, V. Ramaswamy, M. D. Schwarzkopf, G. Stenchikov and R. J. Stouffer (2006). 'Assessment of twentieth-century regional surface temperature trends using the GFDL CM2 coupled models'. *J. Climate*, 19, pp. 1624–1651. DOI: 10.1175/jcli3709.1.

Kovilakam, M., L. W. Thomason, N. Ernest, L. Rieger, A. Bourassa and L. Millán (2020). 'The Global Space-based Stratospheric Aerosol Climatology (version 2.0): 1979–2018'. *Earth Syst. Sci. Data*, 12, pp. 2607–2634. DOI: 10.5194/essd-12-2607-2020.

Kraft, T., O. K. A. Ling, T. Toledo, B. Scheu, S. C. Stähler, J. Clinton and S. Stange (2023). 'An Antipodal Seismic and (Infra)acoustic View from Central Europe on the 15 January 2022 Hunga–Tonga–Hunga–Ha'apai Eruption'. *Seismol. Res. Lett.*, DOI: 10.1785/0220220254.

Kratzmann, D. J., S. Carey, R. Scasso and J.-A. Naranjo (2009). 'Compositional variations and magma mixing in the 1991 eruptions of Hudson volcano, Chile'. *Bull. Volcanol.*, 71, pp. 419–439. DOI: 10.1007/s00445-008-0234-x.

Le Mével, H., C. A. Miller, M. Ribó, S. Cronin and T. Kula (2023). 'The magmatic system under Hunga volcano before and after the 15 January 2022 eruption'. *Sci. Adv.*, 9. DOI: 10.1126/sciadv.adh3156.

Legras, B., C. Duchamp, P. Sellitto, A. Podglajen, E. Carboni, R. Siddans, J.-U. Grooß, S. Khaykin and F. Ploeger (2022). 'The evolution and dynamics of the Hunga Tonga–Hunga Ha'apai sulfate aerosol plume in the stratosphere'. *Atmos. Chem. Phys.*, 22, pp. 14957–14970. DOI: 10.5194/acp-22-14957-2022.

Lestrelin, H., B. Legras, A. Podglajen and M. Salihoglu (2021). 'Smoke-charged vortices in the stratosphere generated by wildfires and their behaviour in both hemispheres: comparing Australia 2020 to Canada 2017'. *Atmos. Chem. Phys.*, 21, pp. 7113–7134. DOI: 10.5194/acp-21-7113-2021.

Li, Y., C. Pedersen, J. Dykema, J.-P. Vernier, S. Vattioni, A. K. Pandit, A. Stenke, E. Asher, T. Thornberry, M. A. Todt et al. (2023). 'In situ measurements of perturbations to stratospheric aerosol and modeled ozone and radiative impacts following the 2021 La Soufrière eruption'. *Atmos. Chem. Phys.*, 23, pp. 15351–15364. DOI: 10.5194/acp-23-15351-2023.

Lopez, T., L. Clarisse, H. Schwaiger, A. Van Eaton, M. Loewen, D. Fee, J. Lyons, K. Wallace, C. Searcy, A. Wech et al. (2020). 'Constraints on eruption processes and event masses for the 2016–2017 eruption of Bogoslof volcano, Alaska, through evaluation of IASI satellite SO_2 masses and complementary datasets'. *Bull. Volcanol.*, 82, 17. DOI: 10.1007/s00445-019-1348-z.

Lynett, P., M. McCann, Z. Zhou, W. Renteria, J. Borrero, D. Greer, O. Fa'anunu, C. Bosserelle, B. Jaffe, S. La Selle et al. (2022). 'Diverse tsunamigenesis triggered by the Hunga Tonga-Hunga Ha'apai eruption'. *Nature*, 609, pp. 728–733. DOI: 10.1038/s41586-022-05170-6.

Lyons, J. J., M. M. Haney, D. Fee, A. G. Wech and C. F. Waythomas (2019). 'Infrasound from giant bubbles during explosive submarine eruptions'. *Nat. Geosci.*, 12, pp. 952–958. DOI: 10.1038/s41561-019-0461-0.

Madden-Nadeau, A. L., M. Cassidy, D. M. Pyle, T. A. Mather, S. F. L. Watt, S. L. Engwell, M. Abdurrachman, M. E. M. Nurshal, D. R. Tappin and T. Ismail (2021). 'The magmatic and eruptive evolution of the 1883 caldera-forming eruption of Krakatau: Integrating field- to crystal-scale observations'. *J. Volcanol. Geotherm. Res.*, 411, 107176. DOI: 10.1016/j.jvolgeores.2021.107176.

Maeno, F., T. Kaneko, M. Ichihara, Y. J. Suzuki, A. Yasuda, K. Nishida and T. Ohminato (2022). 'Seawater-magma interactions sustained the high column during the 2021 phreatomagmatic eruption of Fukutoku-Oka-no-Ba'. *Commun. Earth Environ.*, 3, 260. DOI: 10.1038/s43247-022-00594-4.

Malinina, E., A. Rozanov, U. Niemeier, S. Wallis, C. Arosio, F. Wrana, C. Timmreck, C. von Savigny and J. P. Burrows (2021). 'Changes in stratospheric aerosol extinction coefficient after the 2018 Ambae eruption as seen by OMPS-LP and MAECHAM5-HAM'. *Atmos. Chem. Phys.*, 21, pp. 14871–14891. DOI: 10.5194/acp-21-14871-2021.

Mandeville, C. W., S. Carey and H. Sigurdsson (1996a). 'Magma mixing, fractional crystallization and volatile degassing during the 1883 eruption of Krakatau volcano, Indonesia'. *J. Volcanol. Geotherm. Res.*, 74, pp. 243–274. DOI: 10.1016/s0377-0273(96)00060-1.

Mandeville, C. W., S. Carey and H. Sigurdsson (1996b). 'Sedimentology of the Krakatau 1883 submarine pyroclastic deposits'. *Bull. Volcanol.*, 57, pp. 512–529. DOI: 10.1007/BF00304436.

Mandeville, C. W., S. Carey, H. Sigurdsson and J. King (1994). 'Paleomagnetic evidence for high-temperature emplacement of the 1883 subaqueous pyroclastic flows from Krakatau Volcano, Indonesia'. *J. Geophys. Res.*, 99, pp. 9487–9504. DOI: 10.1029/94JB00239.

Manga, M., K. E. Fauria, C. Lin, S. J. Mitchell, M. P. Jones, C. E. Conway, W. Degruyter, B. Hosseini, R. Carey, R. Cahalan et al. (2018). 'The pumice raft-forming 2012 Havre submarine eruption was effusive'. *Earth Planet. Sci. Lett.*, 489, pp. 49–58. DOI: 10.1016/j.epsl.2018.02.025.

Mastin, L. G., M. Guffanti, R. Servranckx, P. Webley, S. Barsotti, K. Dean, A. Durant, J. W. Ewert, A. Neri, W. I. Rose et al. (2009). 'A multidisciplinary effort to assign realistic source parameters to models of volcanic ash-cloud transport and dispersion during eruptions'. *J. Volcanol. Geotherm. Res.*, 186, pp. 10–21. DOI: 10.1016/j.jvolgeores.2009.01.008.

Mastin, L. G. and J. B. Witter (2000). 'The hazards of eruptions through lakes and seawater'. *J. Volcanol. Geotherm. Res.*, 97, pp. 195–214. DOI: 10.1016/s0377-0273(99)00174-2.

Mastin, L. G., A. R. Van Eaton and S. J. Cronin (2024). 'Did steam boost the height and growth rate of the giant Hunga eruption plume?' *Bull. Volcanol.*, 86, 64. DOI: 10.1007/s00445-024-01749-1.

Matoza, R. S., D. Fee, J. D. Assink, A. M. Iezzi, D. N. Green, K. Kim, L. Toney, T. Lecocq, S. Krishnamoorthy, J.-M. Lalande et al. (2022). 'Atmospheric waves and global seismoacoustic observations of the January 2022 Hunga eruption, Tonga'. *Science*, 377, pp. 95–100. DOI: 10.1126/science.abo7063.

Millán, L., M. L. Santee, A. Lambert, N. J. Livesey, F. Werner, M. J. Schwartz, H. C. Pumphrey, G. L. Manney, Y. Wang, H. Su et al. (2022). 'The Hunga Tonga-Hunga Ha'apai Hydration of the Stratosphere'. *Geophys. Res. Lett.*, 49, e2022GL099381. DOI: 10.1029/2022gl099381.

Murcray, D. G., F. J. Murcray, D. B. Barker and H. J. Mastenbrook (1981). 'Changes in stratospheric water vapor associated with the Mount St. Helens

eruption'. *Science*, 211, pp. 823–824. DOI: 10.1126/science.211.4484.823.

Muser, L. O., G. A. Hoshyaripour, J. Bruckert, Á. Horváth, E. Malinina, S. Wallis, F. J. Prata, A. Rozanov, C. von Savigny, H. Vogel et al. (2020). 'Particle aging and aerosol–radiation interaction affect volcanic plume dispersion: evidence from the Raikoke 2019 eruption'. *Atmos. Chem. Phys.*, 20, pp. 15015–15036. DOI: 10.5194/acp-20-15015-2020.

NASEM (2017). *Volcanic Eruptions and Their Repose, Unrest, Precursors, and Timing*. National Academies Press. DOI: 10.17226/24650.

Newhall, C. and S. Self (1982). 'The volcanic explosivity index (VEI) an estimate of explosive magnitude for historical volcanism'. *J. Geophys. Res.*, 87, pp. 1231–1238. DOI: 10.1029/hg002p0143.

Ohneiser, K., A. Ansmann, B. Kaifler, A. Chudnovsky, B. Barja, D. A. Knopf, N. Kaifler, H. Baars, P. Seifert, D. Villanueva et al. (2022). 'Australian wildfire smoke in the stratosphere: the decay phase in 2020/2021 and impact on ozone depletion'. *Atmos. Chem. Phys.*, 22, pp. 7417–7442. DOI: 10.5194/acp-22-7417-2022.

Ohneiser, K., A. Ansmann, J. Witthuhn, H. Deneke, A. Chudnovsky, G. Walter and F. Senf (2023). 'Self-lofting of wildfire smoke in the troposphere and stratosphere: simulations and space lidar observations'. *Atmos. Chem. Phys.*, 23, pp. 2901–2925. DOI: 10.5194/acp-23-2901-2023.

Oppenheimer, C., T. P. Fischer and B. Scaillet (2014). 'Volcanic Degassing: Process and Impact'. *Treatise on Geochemistry*. Vol. 4. Elsevier, pp. 111–179. DOI: 10.1016/b978-0-08-095975-7.00304-1.

Pernter, J. (1889). 'Der Krakatau-Ausbruch und seine Folge-Erscheinungen'. *Meteorol. Z.*, 6, 457. https://homepages.see.leeds.ac.uk/~amtgwm/Pernter_1889_Pg457.pdf.

Perttu, A., J. Assink, A. R. Van Eaton, C. Caudron, C. Vagasky, J. Krippner, K. McKee, S. De Angelis, B. Perttu, B. Taisne et al. (2023). 'Remote Characterization of the 12 January 2020 Eruption of Taal Volcano, Philippines, Using Seismo-Acoustic, Volcanic Lightning, and Satellite Observations'. *Bull. Seismol. Soc. Am.*, 113, pp. 1471–1492. DOI: 10.1785/0120220223.

Pitari, G. and E. Mancini (2002). 'Short-term climatic impact of the 1991 volcanic eruption of Mt. Pinatubo and effects on atmospheric tracers'. *Nat. Hazards Earth Syst. Sci.*, DOI: 10.5194/nhess-2-91-2002.

Poli, P. and N. M. Shapiro (2022). 'Rapid Characterization of Large Volcanic Eruptions: Measuring the Impulse of the Hunga Tonga Ha'apai Explosion From Teleseismic Waves'. *Geophys. Res. Lett.*, 49, e2022GL098123. DOI: 10.1029/2022GL098123.

Prata, A. T., A. Folch, A. J. Prata, R. Biondi, H. Brenot, C. Cimarelli, S. Corradini, J. Lapierre and A. Costa (2020). 'Anak Krakatau triggers volcanic freezer in the upper troposphere'. *Sci. Rep.*, 10, pp. 1–13. DOI: 10.1038/s41598-020-60465-w.

Prata, A. T., R. G. Grainger, I. A. Taylor, A. C. Povey, S. R. Proud and C. A. Poulsen (2022). 'Uncertainty-bounded estimates of ash cloud properties using the ORAC algorithm: application to the 2019 Raikoke eruption'. *Atmos. Meas. Tech.*, 15, pp. 5985–6010. DOI: 10.5194/amt-15-5985-2022.

Prata, F., A. T. Prata, R. Tanner, R. G. Grainger, M. Borgas and T. J. Aubry (2025). 'The radial spreading of volcanic umbrella clouds deduced from satellite measurements'. *Volcanica*, 8, pp. 1–29. DOI: 10.30909/vol.08.01.0129.

Preine, J., J. Karstens, C. Hübscher, T. Druitt, S. Kutterolf, P. Nomikou, M. Manga, R. Gertisser, K. Pank, S. Beethe et al. (2024). 'Hazardous explosive eruptions of a recharging multi-cyclic island arc caldera'. *Nat. Geosci.*, 17, pp. 323–331. DOI: 10.1038/s41561-024-01392-7.

Proud, S. R., A. T. Prata and S. Schmauß (2022). 'The January 2022 eruption of Hunga Tonga-Hunga Ha'apai volcano reached the mesosphere'. *Science*, 378, pp. 554–557. DOI: 10.1126/science.abo4076.

Purkis, S. J., S. N. Ward, N. M. Fitzpatrick, J. B. Garvin, D. Slayback, S. J. Cronin, M. Palaseanu-Lovejoy and A. Dempsey (2023). 'The 2022 Hunga-Tonga megatsunami: Near-field simulation of a once-in-a-century event'. *Sci. Adv.*, 9, eadf5493. DOI: 10.1126/sciadv.adf5493.

Pyle, D. M. (2015). 'Sizes of Volcanic Eruptions'. *The Encyclopedia of Volcanoes*. Ed. by H. Sigurdsson et al. 2nd. Elsevier, pp. 257–264. DOI: 10.1016/b978-0-12-385938-9.00013-4.

Rampino, M. R. and S. Self (1982). 'Historic Eruptions of Tambora (1815), Krakatau (1883), and Agung (1963), Their Stratospheric Aerosols, and Climatic Impact'. *Quat. Res.*, 18, pp. 127–143. DOI: 10.1016/0033-5894(82)90065-5.

Ringler, A. T., R. E. Anthony, R. C. Aster, T. Taira, B. R. Shiro, D. C. Wilson, S. De Angelis, C. Ebeling, M. Haney, R. S. Matoza et al. (2023). 'The global seismographic network reveals atmospherically coupled

normal modes excited by the 2022 Hunga Tonga eruption'. *Geophys. J. Int.*, 232, pp. 2160–2174. DOI: 10.1093/gji/ggac284.

Rose, W. I., D. J. Delene, D. J. Schneider, G. J. S. Bluth, A. J. Krueger, I. Sprod, C. McKee, H. L. Davies and G. G. J. Ernst (1995). 'Ice in the 1994 Rabaul eruption cloud: implications for volcano hazard and atmospheric effects'. *Nature*, 375, pp. 477–479. DOI: 10.1038/375477a0.

Rowell, C. R., A. M. Jellinek, S. Hajimirza and T. J. Aubry (2022). 'External Surface Water Influence on Explosive Eruption Dynamics, With Implications for Stratospheric Sulfur Delivery and Volcano-Climate Feedback'. *Front. Earth Sci.*, 10, 788294. DOI: 10.3389/feart.2022.788294.

Scaillet, B., J. F. Luhr and M. R. Carroll (2003). 'Petrological and Volcanological Constraints on Volcanic Sulfur Emissions to the Atmosphere'. *Volcanism and the Earth's Atmosphere*. Vol. 139. Geophysical Monograph. American Geophysical Union, pp. 11–40. DOI: 10.1029/139GM02.

Schoeberl, M. R., Y. Wang, G. Taha, D. J. Zawada, R. Ueyama and A. Dessler (2024). 'Evolution of the Climate Forcing During the Two Years After the Hunga Tonga-Hunga Ha'apai Eruption'. *J. Geophys. Res.*, 129, e2024JD041296. DOI: 10.1029/2024jd041296.

Scott, W. E. et al. (1996). 'Pyroclastic Flows of the June 15, 1991, Climactic Eruption of Mount Pinatubo'. *Fire and Mud: Eruptions and Lahars of Mount Pinatubo, Philippines*. Ed. by C. Newhall and R. Punongbayan. https://pubs.usgs.gov/pinatubo/index.html. Seattle, USA: University of Washington Press.

Seabrook, S., K. Mackay, S. J. Watson, M. A. Clare, J. E. Hunt, I. A. Yeo, E. M. Lane, M. R. Clark, R. Wysoczanski, A. A. Rowden et al. (2023). 'Volcaniclastic density currents explain widespread and diverse seafloor impacts of the 2022 Hunga Volcano eruption'. *Nat. Commun.*, 14, 7881. DOI: 10.1038/s41467-023-43607-2.

Self, S. (1992). 'Krakatau revisited: the course of events and interpretation of the 1883 eruption'. *GeoJournal*, 28, pp. 109–121. DOI: 10.1007/BF00177223.

Self, S. and M. R. Rampino (1981). 'The 1883 eruption of Krakatau'. *Nature*, 294, pp. 699–704. DOI: 10.1038/294699a0.

Self, S. and R. S. J. Sparks (1978). 'Characteristics of widespread pyroclastic deposits formed by the interaction of silicic magma and water'. *Bull. Volcanol.*, 41, pp. 196–212. DOI: 10.1007/bf02597223.

Sellitto, P., A. Podglajen, R. Belhadji, M. Boichu, E. Carboni, J. Cuesta, C. Duchamp, C. Kloss, R. Siddans, N. Bègue et al. (2022). 'The unexpected radiative impact of the Hunga Tonga eruption of 15th January 2022'. *Commun. Earth Environ.*, 3, 288. DOI: 10.1038/s43247-022-00618-z.

Sellitto, P., R. Siddans, R. Belhadji, E. Carboni, B. Legras, A. Podglajen and et al. (2024). 'Observing the SO_2 and sulfate aerosol plumes from the 2022 Hunga eruption with the Infrared Atmospheric Sounding Interferometer (IASI)'. *Geophys. Res. Lett.*, 51, e2023GL105565. DOI: 10.1029/2023GL105565.

Sigl, M., M. Winstrup, J. R. McConnell, K. C. Welten, G. Plunkett, F. Ludlow, U. Büntgen, M. Caffee, N. Chellman, D. Dahl-Jensen et al. (2015). 'Timing and climate forcing of volcanic eruptions for the past 2,500 years'. *Nature*, 523, pp. 543–549. DOI: 10.1038/nature14565.

Sigurdsson, H., S. Carey, C. W. Mandeville and S. Bronto (1991). 'Pyroclastic Flows of the 1883 Krakatau Eruption'. *Eos*, 72. DOI: 10.1029/90EO00286.

Sioris, C. E., A. Malo, C. A. McLinden and R. D'Amours (2016). 'Direct injection of water vapor into the stratosphere by volcanic eruptions'. *Geophys. Res. Lett.*, 43, pp. 7694–7700. DOI: 10.1002/2016GL069918.

Solomon, S., K. Dube, K. Stone, P. Yu, D. Kinnison, O. B. Toon, S. E. Strahan, K. H. Rosenlof, R. Portmann, S. Davis et al. (2022). 'On the stratospheric chemistry of midlatitude wildfire smoke'. *Proc. Natl. Acad. Sci.*, 119, e2117325119. DOI: 10.1073/pnas.2117325119.

Souza, G., J.-P. Vernier, D. Quintão, B. Biazon, F. Lopes, J. Ricardo, A. K. Pandit, R. C. Das, H. Liu, T. N. N. Knepp et al. (2025). 'Sedimentation and growth of volcanic aerosols within the Hunga plume: Insights from unique tropical in situ and satellite measurements'. *ESS Open Archive*, DOI: 10.22541/essoar.174241613.36494891/v1.

Sparks, R. S. J. et al. (1997). *Volcanic Plumes (Chapter 8: Submarine volcanism and hydrovolcanism)*. John Wiley & Sons, Inc., p. 557.

Stone, K. A., S. Solomon, D. E. Kinnison, M. C. Pitts, L. R. Poole, M. J. Mills, A. Schmidt, R. R. Neely, D. Ivy, M. J. Schwartz et al. (2017). 'Observing the impact of Calbuco volcanic aerosols on south polar ozone depletion in 2015'. *J. Geophys. Res.*, 122, pp. 11862–11879. DOI: 10.1002/2017JD026987.

Symons, G. J. et al., eds. (1888). *The Eruption of Krakatoa and Subsequent Phenomena: report of the Krakatoa committee of the Royal Society*. UK: Trübner & Company, p. 494.

Taha, G., R. Loughman, P. R. Colarco, T. Zhu, L. W. Thomason and G. Jaross (2022). 'Tracking the 2022 Hunga Tonga-Hunga Ha'apai Aerosol Cloud in the Upper and Middle Stratosphere Using Space-Based Observations'. *Geophys. Res. Lett.*, 49, e2022GL100091. DOI: 10.1029/2022gl100091.

Taha, G., R. Loughman, T. Zhu, L. Thomason, J. Kar, L. Rieger and A. Bourassa (2021). 'OMPS LP Version 2.0 multi-wavelength aerosol extinction coefficient retrieval algorithm'. *Atmos. Meas. Tech.*, 14, pp. 1015–1036. DOI: 10.5194/amt-14-1015-2021.

Taylor, I. A., R. G. Grainger, A. T. Prata, S. R. Proud, T. A. Mather and D. M. Pyle (2023). 'A satellite chronology of plumes from the April 2021 eruption of La Soufrière, St Vincent'. *Atmos. Chem. Phys.*, 23, pp. 15209–15234. DOI: 10.5194/acp-23-15209-2023.

Thurin, J., C. Tape and R. Modrak (2022). 'Multi-Event Explosive Seismic Source for the 2022 Mw 6.3 Hunga Tonga Submarine Volcanic Eruption'. *The Seismic Record*, 2, pp. 217–226. DOI: 10.1785/0320220027.

Tilling, R. I., L. Topinka and D. A. Swanson, eds. (1990). *Eruptions of Mount St. Helens: Past, Present, and Future*. Denver, CO: U.S. Geological Survey. DOI: 10.3133/7000008.

Toohey, M. and M. Sigl (2017). 'Volcanic stratospheric sulfur injections and aerosol optical depth from 500 BCE to 1900 CE'. *Earth Syst. Sci. Data*, 9, pp. 809–831. DOI: 10.5194/essd-9-809-2017.

Ulvrova, M., R. Paris, P. Nomikou, K. Kelfoun, S. Leibrandt, D. Tappin and F. McCoy (2016). 'Source of the tsunami generated by the 1650 AD eruption of Kolumbo submarine volcano (Aegean Sea, Greece)'. *J. Volcanol. Geotherm. Res.*, 321, pp. 125–139. DOI: 10.1016/j.jvolgeores.2016.04.034.

Valentine, G. (1993). 'Role of magma-water interaction in very large explosive eruptions'. *International Seminar on Physics of Vapor Explosion (Proceedings)*. https://www.osti.gov/biblio/144909. Tomakomai, Hokkaido, Japan, pp. 210–216.

Van Eaton, A. R., M. Herzog, C. J. N. Wilson and J. McGregor (2012). 'Ascent dynamics of large phreatomagmatic eruption clouds: The role of microphysics'. *J. Geophys. Res.*, 117, B03203. DOI: 10.1029/2011jb008892.

Van Eaton, A. R., J. Lapierre, S. A. Behnke, C. Vagasky, C. J. Schultz, M. Pavolonis, K. Bedka and K. Khlopenkov (2023). 'Lightning Rings and Gravity Waves: Insights Into the Giant Eruption Plume From Tonga's Hunga Volcano on 15 January 2022'. *Geophys. Res. Lett.*, 50, e2022GL102341. DOI: 10.1029/2022gl102341.

Van Eaton, A. R., C. M. Smith, M. Pavolonis and R. Said (2022). 'Eruption dynamics leading to a volcanic thunderstorm—The January 2020 eruption of Taal volcano, Philippines'. *Geology*, 50, pp. 491–495. DOI: 10.1130/g49490.1.

Vaughan, R. G. and P. W. Webley (2010). 'Satellite observations of a surtseyan eruption: Hunga Ha'apai, Tonga'. *J. Volcanol. Geotherm. Res.*, 198, pp. 177–186. DOI: 10.1016/j.jvolgeores.2010.08.017.

Verbeek, R. D. M. (1884). 'The Krakatoa Eruption'. *Nature*, 30, pp. 10–15. DOI: 10.1038/030010a0.

Verbeek, R. D. M. (1885). *Krakatau*. Batavia, p. 614. DOI: 10.2307/196734.

Vergoz, J., P. Hupe, C. Listowski, A. Le Pichon, M. A. Garcés, E. Marchetti, P. Labazuy, L. Ceranna, C. Pilger, P. Gaebler et al. (2022). 'IMS observations of infrasound and acoustic-gravity waves produced by the January 2022 volcanic eruption of Hunga, Tonga: A global analysis'. *Earth Planet. Sci. Lett.*, 591, 117639. DOI: 10.1016/j.epsl.2022.117639.

Vernier, H., D. Quintão, B. Biazon, E. Landulfo, G. Souza, V. A. Santos, J. S. F. Lopes, C. P. A. Mendes, A. S. J. D. Matta, K. P. Damaris et al. (2025). 'Balloon Observations Suggesting Sea Salt Injection into the Stratosphere from Hunga Tonga-Hunga Ha'apai'. DOI: 10.5194/egusphere-2025-924.

Vernier, J.-P., T. J. Aubry, C. Timmreck, A. Schmidt, L. Clarisse, F. Prata, N. Theys, A. T. Prata, G. Mann, H. Choi et al. (2024). 'The 2019 Raikoke eruption as a testbed used by the Volcano Response group for rapid assessment of volcanic atmospheric impacts'. *Atmos. Chem. Phys.*, 24, pp. 5765–5782. DOI: 10.5194/acp-24-5765-2024.

Vernier, J.-P., T. D. Fairlie, T. Deshler, M. Natarajan, T. Knepp, K. Foster, F. G. Wienhold, K. M. Bedka, L. Thomason and C. Trepte (2016). 'In situ and space-based observations of the Kelud volcanic plume: the persistence of ash in the lower stratosphere'. *J. Geophys. Res.*, 121, pp. 11104–11118. DOI: 10.1002/2016jd025344.

Walker, G. P. L. (1973). 'Explosive volcanic eruptions — a new classification scheme'. *Geol. Rundschau*, 62, pp. 431–446. DOI: 10.1007/bf01840108.

Walker, G. P. L. (1979). 'A volcanic ash generated by explosions where ignimbrite entered the sea'. *Nature*, 281, pp. 642–646. DOI: 10.1038/281642a0.

Walker, S. L. and C. E. J. de Ronde (2024). 'Ongoing activity at Hunga submarine volcano, Tonga: The case for better monitoring of submarine volcanoes worldwide'. *Geochem. Geophys. Geosyst.*, 25, e2024GC011685. DOI: 10.1029/2024GC011685.

Wei, L., X. Pan, E. Trasatti, M. Ao, S. Liu, C. Tolomei, G. Liu and G. Ventura (2025). 'Deformation and morphological changes before the 2021–2022 explosive eruption at Hunga Tonga-Hunga Ha'apai submarine caldera revealed by satellite remote sensing'. *Bull. Volcanol.*, 87, 17. DOI: 10.1007/s00445-025-01804-5.

Wexler, H. (1951). 'Spread of the Krakatoa volcanic dust cloud as related to the high-level circulation'. *Bull. Am. Meteorol. Soc.*, 32, pp. 48–51. DOI: 10.1175/1520-0477-32.2.48.

White, J. D. L., C. I. Schipper and K. Kano (2015). 'Submarine Explosive Eruptions'. *Encyclopedia of Volcanoes, 2nd Ed.* Pp. 553–570. DOI: 10.1016/b978-0-12-385938-9.00031-6.

Wright, C. J., N. P. Hindley, M. J. Alexander, M. Barlow, L. Hoffmann, C. N. Mitchell, F. Prata, M. Bouillon, J. Carstens, C. Clerbaux et al. (2022). 'Surface-to-space atmospheric waves from Hunga Tonga-Hunga Ha'apai eruption'. *Nature*, 609, pp. 741–746. DOI: 10.1038/s41586-022-05012-5.

Wu, J., S. J. Cronin, M. Brenna, S.-H. Park, A. Pontesilli, I. A. Ukstins, D. Adams, J. Paredes-Mariño, K. Hamilton, M. Huebsch et al. (2025). 'Low sulfur emissions from 2022 Hunga eruption due to seawater–magma interactions'. *Nat. Geosci.*, 18, pp. 518–524. DOI: 10.1038/s41561-025-01691-7.

Yeo, I. A., I. M. McIntosh, S. E. Bryan, K. Tani, M. Dunbabin, K. J. Dobson, S. J. Mitchell, P. C. Collins, M. A. Clare, H. Cathey et al. (2024). 'The 2019 pumice raft forming eruption of Volcano-F (Volcano 0403–091) and implications for hazards posed by submerged calderas'. *J. Volcanol. Geotherm. Res.*, 454, 108160. DOI: 10.1016/j.jvolgeores.2024.108160.

Yu, P., S. M. Davis, O. B. Toon, R. W. Portmann, C. G. Bardeen, J. E. Barnes, H. Telg, C. Maloney and K. H. Rosenlof (2021). 'Persistent stratospheric warming due to 2019–2020 Australian wildfire smoke'. *Geophys. Res. Lett.*, 48, e2021GL092609. DOI: 10.1029/2021GL092609.

Yu, P., O. B. Toon, C. G. Bardeen, Y. Zhu, K. H. Rosenlof, R. W. Portmann, T. D. Thornberry, R.-S. Gao, S. M. Davis, E. T. Wolf et al. (2019). 'Black carbon lofts wildfire smoke high into the stratosphere to form a persistent plume'. *Science*, 365, pp. 587–590. DOI: 10.1126/science.aax1748.

Zhu, Y., C. G. Bardeen, S. Tilmes, M. J. Mills, X. Wang, V. L. Harvey, G. Taha, D. Kinnison, R. W. Portmann, P. Yu et al. (2022). 'Perturbations in stratospheric aerosol evolution due to the water-rich plume of the 2022 Hunga-Tonga eruption'. *Commun. Earth Environ.*, 3, 248. DOI: 10.1038/s43247-022-00580-w.

Zhu, Y., O. B. Toon, E. J. Jensen, C. G. Bardeen, M. J. Mills, M. A. Tolbert, P. Yu and S. Woods (2020). 'Persisting volcanic ash particles impact stratospheric SO2 lifetime and aerosol optical properties'. *Nat. Commun.*, 11, 4526. DOI: 10.1038/s41467-020-18352-5.

Zhu, Y., O. B. Toon, D. Kinnison, V. L. Harvey, M. J. Mills, C. G. Bardeen, M. Pitts, N. Bègue, J.-B. Renard, G. Berthet et al. (2018). 'Stratospheric aerosols, polar stratospheric clouds, and polar ozone depletion after the Mount Calbuco eruption in 2015'. *J. Geophys. Res.*, 123, pp. 12308–12331. DOI: 10.1029/2018JD028974.

Zielinski, G. A. (1995). 'Stratospheric loading and optical depth estimates of explosive volcanism over the last 2100 years derived from the Greenland Ice Sheet Project 2 ice core'. *J. Geophys. Res.*, 100, pp. 20937–20955. DOI: 10.1029/95jd01751.

Zimanowski, B., R. Büttner, P. Dellino, J. D. L. White and K. H. Wohletz (2015). 'Magma-Water Interaction and Phreatomagmatic Fragmentation'. *Encyclopedia of Volcanoes, 2nd Ed.* Pp. 473–484. DOI: 10.1016/B978-0-12-385938-9.00026-2.